

Circulation Research

JOURNAL OF THE AMERICAN HEART ASSOCIATION



Simulation Study of Cellular Electric Properties in Heart Failure

Leo Priebe and Dirk J. Beuckelmann

Circ. Res. 1998;82;1206-1223

Circulation Research is published by the American Heart Association, 7272 Greenville Avenue, Dallas, TX 75214

Copyright © 1998 American Heart Association. All rights reserved. Print ISSN: 0009-7330. Online ISSN: 1524-4571

The online version of this article, along with updated information and services, is located on the World Wide Web at:

<http://circres.ahajournals.org/cgi/content/full/82/11/1206>

Subscriptions: Information about subscribing to Circulation Research is online at
<http://circres.ahajournals.org/subscriptions/>

Permissions: Permissions & Rights Desk, Lippincott Williams & Wilkins, a division of Wolters Kluwer Health, 351 West Camden Street, Baltimore, MD 21202-2436. Phone: 410-528-4050. Fax: 410-528-8550. E-mail:
journalpermissions@lww.com

Reprints: Information about reprints can be found online at
<http://www.lww.com/reprints>

Simulation Study of Cellular Electric Properties in Heart Failure

Leo Priebe, Dirk J. Beuckelmann

Abstract—Patients with severe heart failure are at high risk of sudden cardiac death. In the majority of these patients, sudden cardiac death is thought to be due to ventricular tachyarrhythmias. Alterations of the electric properties of single myocytes in heart failure may favor the occurrence of ventricular arrhythmias in these patients by inducing early or delayed afterdepolarizations. Mathematical models of the cellular action potential and its underlying ionic currents could help to elucidate possible arrhythmogenic mechanisms on a cellular level. In the present study, selected ionic currents based on human data are incorporated into a model of the ventricular action potential for the purpose of studying the cellular electrophysiological consequences of heart failure. Ionic currents that are not yet sufficiently characterized in human ventricular myocytes are adopted from the action potential model developed by Luo and Rudy (LR model). The main results obtained from this model are as follows: The action potential in ventricular myocytes from failing hearts is longer than in nonfailing control hearts. The major underlying mechanisms for this prolongation are the enhanced activity of the Na^+ - Ca^{2+} exchanger, the slowed diastolic decay of the $[\text{Ca}^{2+}]_i$ transient, and the reduction of the inwardly rectifying K^+ current and the Na^+ - K^+ pump current in myocytes of failing hearts. Furthermore, the fast and slow components of the delayed rectifier K^+ current (I_{Kr} and I_{Ks} , respectively) are of utmost importance in determining repolarization of the human ventricular action potential. In contrast, the influence of the transient outward K^+ current on APD is only small in both cell groups. Inhibition of I_{Kr} promotes the development of early afterdepolarizations in failing, but not nonfailing, myocytes. Furthermore, spontaneous Ca^{2+} release from the sarcoplasmic reticulum triggers a premature action potential only in failing myocytes. This model of the ventricular action potential and its alterations in heart failure is intended to serve as a tool for investigating the effects of therapeutic interventions on the electric excitability of the human ventricular myocardium. (*Circ Res.* 1998;82:1206-1223.)

Key Words: action potential ■ computer model ■ arrhythmia ■ heart failure

Patients with severe heart failure are at high risk of sudden cardiac death. More than 50% of these patients die suddenly.¹ In the majority of these patients, sudden cardiac death is thought to be due to ventricular tachyarrhythmias. The mechanisms underlying these lethal arrhythmias are largely unknown. However, in animal models of heart failure and in humans, there is evidence that reentry as well as nonreentrant mechanisms may play a role.²⁻⁴ Triggered activity arising from EADs or DADs and abnormal automaticity are possible cellular mechanisms underlying nonreentrant arrhythmias.⁵⁻⁸ In animal studies, Ca^{2+} influx through voltage-gated I_{Ca} was demonstrated to cause EADs.^{9,10} Cation influx through $I_{\text{ns(Ca)}}$ or Na^+ influx via the electrogenic I_{NaCa} was found to underlie DADs.^{11,12} However, it is unknown what influence these currents may have on triggered activity in human ventricular myocardium. In recent years, quantitative studies of ionic currents in human ventricular cells have greatly enlarged our knowledge about the characteristics of the human AP in patients with and without heart failure.¹³⁻²⁵ In some of these studies, great variations in shape and duration of the APs have been found. Nevertheless, an

unequivocal result was that the AP is prolonged in human ventricular myocytes isolated from patients with heart failure compared with control subjects. Various ionic currents have been shown to be altered in heart failure. I_{K1} ^{13,22} and I_{to} ^{13,19} have been found to be reduced by some groups, although this finding was not undisputed. Wettwer et al¹⁴ have found no significant alterations in current densities and kinetics of I_{to} in failing compared with nonfailing myocytes. Current densities and kinetics of I_{Ca} , however, have been shown to be unaltered by most groups.^{15,16,18}

A prominent feature of the single myocyte of the failing heart is an alteration of $[\text{Ca}^{2+}]_i$ handling^{26,27} and an enhanced activity of the Na^+ - Ca^{2+} exchanger.^{28,29} It has been postulated that these abnormalities may give rise to arrhythmias in heart failure, but proof for this hypothesis remains lacking. Mathematical models of the cellular AP and its underlying ionic currents may help to elucidate possible arrhythmogenic mechanisms on a cellular level. For this purpose, a model of the ventricular AP based on Hodgkin-Huxley formalisms³⁰ was developed. Selected depolarizing and repolarizing ionic currents and the $[\text{Ca}^{2+}]_i$ handling incorporated into this model

Received January 5, 1998; accepted April 6, 1998.

From the Department of Medicine III, University of Cologne, Cologne, Germany.

Correspondence to Dirk J. Beuckelmann, MD, University of Cologne, Department of Medicine III, Joseph-Stelzmann-Str.9, D-50924 Cologne, Germany. E-mail Dirk.Beuckelmann@uni-koeln.de

© 1998 American Heart Association, Inc.

Selected Abbreviations and Acronyms

[A]	= maximum concentration of [A]
AP	= action potential
APD	= action potential duration
APD ₂₅ , APD ₅₀ , APD ₉₀	= APD at 25%, 50%, and 90% repolarization
CICR	= Ca ²⁺ -induced Ca ²⁺ release
DAD	= delayed afterdepolarization
EAD	= early afterdepolarization
g _{max}	= maximal conductance
I _{Ca}	= L-type Ca ²⁺ current
I _{Ca,b}	= Ca ²⁺ background current
I _K	= delayed rectifier K ⁺ current
I _{K1}	= inward rectifier K ⁺ current
I _{Kr} , I _{Ks}	= rapid and slow component of I _K
I _{Ktail}	= K ⁺ tail current
I _{Na}	= fast Na ⁺ current
I _{Na,b}	= Na ⁺ background current
I _{NaCa}	= Na ⁺ -Ca ²⁺ exchanger current
I _{NaK}	= Na ⁺ -K ⁺ pump current
I _{ns(Ca)}	= Ca ²⁺ -dependent nonspecific cation current
I _{st}	= stimulus current
I _{to}	= transient outward K ⁺ current
JSR	= junctional sarcoplasmic reticulum
k	= slope factor
K _{leak}	= rate of Ca ²⁺ leakage out of NSR
K _{mi}	= half-saturation concentration of channel i
k _{NaCa}	= scaling factor of I _{NaCa}
LR	= Luo-Rudy
NSR	= network sarcoplasmic reticulum
SR	= sarcoplasmic reticulum
V _{0.5}	= 50% activation voltage

were based on quantitative measurements in single ventricular myocytes isolated from nonfailing and terminally failing human hearts.

Using this model, we evaluated which ionic currents may affect the AP in human myocardium and which cellular abnormalities in human ventricular myocytes from failing hearts may contribute to arrhythmogenesis in heart failure.

Materials and Methods

A variety of ionic currents and electrogenic ion pumps and exchangers that have been described in animals have not been sufficiently characterized in human ventricular myocytes. Therefore, these currents have to be calculated by equations used in an AP model developed for guinea pig ventricular myocytes by Luo and Rudy³¹ (LR model). However, the major ionic currents, I_{Ca}, I_{to}, I_K with its two components (I_{Kr} and I_{Ks}), and I_{K1}, are based on human data. In addition, the [Ca²⁺]_i transients in human myocytes and their alterations in failing myocytes observed experimentally²⁷ can be simulated by this model. The other currents included into the model, I_{Na}, I_{NaCa}, and I_{NaK}, have to be adopted from the LR model and modulated in such a way that simulations are widely consistent with available human data.

Voltage-clamp data for I_{Ca}, I_{to}, and I_{K1} and Ca²⁺ measurements are as described in our previous studies.^{13,16,19,20,27} Experiments were carried out at 37°C. (See References 13, 16, 19, 20, and 27 for a detailed description of the experimental conditions.)

Under space-clamp conditions, the differential equation describing the time-dependent changes in membrane potential (V) is as follows:

$$dV/dt = -(1/C_m)(I_{Na} + I_{Ca} + I_{to} + I_{Kr} + I_{Ks} + I_{K1} + I_{NaCa} + I_{NaK} + I_{Na,b} + I_{Ca,b} + I_{st})$$

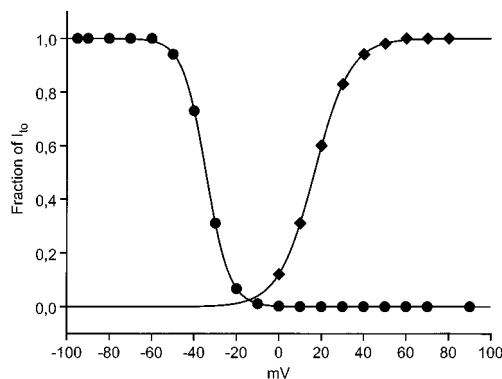


Figure 1. Steady-state activation (◆) and inactivation (●) of simulated I_{to} at indicated voltages. Computed curves are a Boltzmann fit to the data according to the following equation: $I/I_{max} = I_{max} / \{1 + \exp[(v - V_{0.5})/k]\}$, where I indicates current, and v is the membrane potential.

where C_m is the membrane capacitance and I_{st} is an externally applied stimulus current. The ionic currents I_x are calculated by ionic gates using Hodgkin-Huxley-type formalisms.³⁰ All ionic currents are computed for 1 pF of cell membrane capacitance.

The complete set of equations of all ionic currents, ionic exchanger currents, and [Ca²⁺]_i handling is provided in the Appendix.

Fast Na⁺ Current: I_{Na}

I_{Na} is calculated using equations of the LR model.³¹ Sakakibara et al²⁵ have demonstrated that the characteristics of I_{Na} in isolated human ventricular myocytes are similar to those of other mammalian species and that I_{Na} kinetics are identical in several different disease states. Therefore, we use the same equations for I_{Na} in both cell groups.

L-Type Ca²⁺ Current: I_{Ca}

The kinetics of I_{Ca} have been shown to be unaltered in myocytes from failing hearts.^{15,16,18} Therefore, for calculating I_{Ca} the same gating parameters are used in both groups. In animal and human studies, it has been clearly demonstrated that the inactivation of I_{Ca} is voltage dependent. In addition, there is experimental evidence indicating that inactivation of I_{Ca} is also Ca²⁺ dependent.^{32,33} This type of regulation of I_{Ca} seems also to exist in human ventricular myocytes.¹⁷ Consequently, we integrate a proportional factor, f_{Ca}, in the equation of I_{Ca} that is formulated as follows: $f_{Ca} = [1 + ([Ca^{2+}]_i / 600 \text{ nmol/L})]^{-1}$. Fitting of experimental I_{Ca} is performed with simulated [Ca²⁺]_i transients formulated as follows: $A \cdot [\exp(-t/\tau_1) - \exp(-t/\tau_2)] + R$. A is a proportional factor, τ₁ and τ₂ are time constants, and R is the basal Ca²⁺ level. By this approach, the important Ca²⁺-dependent inactivation of I_{Ca} may be sufficiently incorporated into this model as the simulations of I_{Ca} indicate.

Transient Outward K⁺ Current: I_{to}

No significant alterations of the kinetics of I_{to} have been found in failing compared with control myocytes.¹⁴ Therefore, the same gating parameters for simulating I_{to} are used in both groups. On the basis of experimental data,²⁰ the current density of I_{to} is assumed to be 64% of the value measured in nonfailing myocytes. The steady-state activation and inactivation curves of I_{to} obtained from fitting the experimental voltage clamp traces are shown in Figure 1.

Data are fitted by a Boltzmann distribution. The parameters V_{0.5} and k of the Boltzmann equation in the model are compared with those from experimental voltage-clamp studies (Table 1). The differences are negligible and can be explained by the different solutions used in the experiments to block interfering currents.

Delayed Rectifier K⁺ Current: I_K

The existence of two components of the delayed rectifier, a rapidly activating component (I_{Kr}) and a slowly activating component (I_{Ks}),

TABLE 1. Parameters of Steady-State Activation and Inactivation of I_{to} (Experimental Data and Model)

Studies	Steady-State Activation		Steady-State Inactivation	
	$V_{0.5}$, mV	k , mV	$V_{0.5}$, mV	k , mV
Wettwer et al ¹⁴	+9.2±1.8	-13.0±0.6	-34.1±2.0	+4.5±0.2
Näbauer et al ¹⁹	+16.7±1.6	-8.4±0.43	-34.5±2.3	+5.5±0.5
Model	+16.7	-8.4	-34.4	+5.6

has been documented by Li et al.²¹ On the basis of their data, both currents are incorporated into the model. The method for simulating I_{Kr} in human ventricular myocytes is the same as that used by Sanguinetti and Jurkiewicz³⁴ in guinea pig myocytes. For simplification, the slow inactivation of I_{Kr} during depolarization at +50 mV observed experimentally (Li et al²¹) is not considered. Quantitative values of I_{Ks} are calculated by fitting the experimental voltage-clamp traces recorded in the study of Li et al to a single exponential function. On depolarization, the activation of I_{Ks} in human ventricular myocytes follows a sigmoidal time course, as has been reported in guinea pig ventricular myocytes.³⁴ This strong sigmoidal activation has also been found in wild-type I_{Ks} .³⁵ Therefore, the second power of activation in the Hodgkin-Huxley formalism of I_{Ks} is used to obtain an adequate fit to the measured traces. In animal studies, I_{Ks} has been shown to be sensitive to intracellular Ca^{2+} ,^{36,37} and I_{Kr} has been shown to be sensitive to extracellular K^+ .³⁷ In the only study investigating I_{Ks} and I_{Kr} in human ventricular myocytes (ie, that of Li et al²¹), experiments were performed only with 5.0 mmol/L EGTA in the pipette solution and with one extracellular K^+ concentration. Thus, it is unclear whether this type of regulation found in animal ventricular myocytes also exists in human ventricular myocytes. Consequently, we do not consider such a regulation of I_{Ks} and I_{Kr} in our model. At the present time, the properties of I_{Kr} and I_{Ks} in heart failure are unknown. Therefore, we assume that I_{Ks} and I_{Kr} are unchanged in heart failure.

Inward Rectifier K^+ Current: I_{K1}

The simulated current density of I_{K1} is assumed to be reduced by 25% at -70 mV in the failing myocyte compared with control myocytes on the basis of results of experimental studies.^{13,22} Since the time-dependent inactivation of I_{K1} can be observed only at voltages negative to -110 mV,²² I_{K1} is assumed to be time independent. As in animal ventricular myocytes, I_{K1} is also almost solely carried by K^+ ions in human ventricular myocytes.²² Therefore, the reversal potential of I_{K1} is calculated by Nernst's equation for K^+ .

Na^+ - Ca^{2+} Exchanger Current: I_{NaCa}

I_{NaCa} is integrated into the model using values from the LR model because data in human ventricular myocytes are not available at present. To compute I_{NaCa} in a nonfailing myocyte, only k_{NaCa} is changed to 50% of the value used in the LR model, taking into account the smaller activity of I_{NaCa} in human myocytes compared with different animal species.³⁸ With such a value of k_{NaCa} , I_{NaCa} simulated in a nonfailing myocyte with a protocol similar to that in experiments by Sham et al³⁸ is in the range of the experimental data (model, 0.50 pA/pF; experiment, 0.54±0.1 pA/pF). In a failing myocyte, we assume 65% greater I_{NaCa} than in a nonfailing myocyte. This assumption is based on the observation of an increase of Na^+ - Ca^{2+} exchanger activity in myocardium from patients with heart failure.²⁸

Na^+ - K^+ Pump Current: I_{NaK}

For simulation of I_{NaK} , we use the equation of the LR model. The magnitude of I_{NaK} has been chosen in a way such that APD in a nonfailing myocyte at a stimulation frequency of 1 Hz is in the range measured experimentally in single human myocytes from nonfailing heart by our group (unpublished data) and by Peeters et al.³⁹ There is a report suggesting that the concentration of the Na^+ , K^+ -ATPase is

decreased by 42% in failing hearts.⁴⁰ This alteration is assumed to represent a proportional decrease in I_{NaK} . Therefore, a 42% reduction in I_{NaK} of a failing myocyte is incorporated into the model.

$[Ca^{2+}]_i$ Transient

To simulate the $[Ca^{2+}]_i$ transients in both groups, the approach of the LR model has been chosen.³¹ In some equations for calculating the Ca^{2+} homeostasis, the parameters are changed in a way such that simulated $[Ca^{2+}]_i$ transients closely resemble those measured in nonfailing and failing human ventricular myocytes.²⁷ The differences in simulations of the intracellular Ca^{2+} fluxes to the LR model are described below. For more details, see Reference 31.

CICR by the SR

The threshold for CICR from the cardiac SR is reduced from 0.18 to 0.005 μ mol/L because of the smaller size of the peak I_{Ca} in human compared with animal myocytes. The time constants for the activation and deactivation of the release process is set to 4 ms. Experimental studies have revealed that the function and number of the ryanodine channels are widely unaltered in heart failure.^{41,42} Therefore, the CICR mechanism is assumed to be equal in nonfailing and failing myocytes.

Ca^{2+} Buffers in the Myoplasm and the SR

There are reports that the affinity of troponin C to Ca^{2+} is unaltered in heart failure.⁴³ Consequently, because of the great contribution of troponin C to the total myoplasmic Ca^{2+} buffer capacity, we have used equal myoplasmic buffer concentrations in nonfailing and failing myocytes. For simulating the Ca^{2+} buffering in the JSR (calsequestrin), we adopted the values of the LR model for our model. There is no evidence of differences in the level of calsequestrin in heart failure.⁴⁴ Therefore, equal concentrations of calsequestrin have been used in both cell groups. With the approach of Hilgemann and Noble,⁴⁵ we compute the steady-state buffering process numerically by using Newton's iterative method.

Ca^{2+} Uptake and Leakage by the NSR

Reduction of the activity of Ca^{2+} -ATPase of the SR in heart failure, as shown in experimental studies,^{46,47} is integrated into the model. To obtain the characteristic Ca^{2+} transients in both cell groups, the scaling factor for Ca^{2+} uptake, \bar{I}_{up} , is set to 0.0045 mmol/(L · ms) in a nonfailing and 0.0015 mmol/(L · ms) in failing myocytes. The K_{leak} value in both cell groups was chosen in way such that Ca^{2+} leakage out of the NSR is equal to the Ca^{2+} uptake in the NSR at basal $[Ca^{2+}]_i$ (nonfailing, $K_{leak}=0.00026$ ms⁻¹; failing, $K_{leak}=0.00017$ ms⁻¹).

Sarcolemmal Ca^{2+} Pump

The contribution of the sarcolemmal Ca^{2+} pump to the extrusion of Ca^{2+} out of the cell has been shown to be very small.⁴⁸ Therefore, we do not consider this pump in our model.

Background Currents

A linear Ca^{2+} background current, $I_{Ca,b}$, is incorporated into the model for balancing the Ca^{2+} extrusion through I_{NaCa} at resting potential in both cell groups. By this mechanism, the resting level of $[Ca^{2+}]_i$ is maintained at 0.12 μ mol/L in a nonfailing myocyte and at 0.15 μ mol/L in a failing myocyte.

A linear Na^+ background current, $I_{Na,b}$, is also incorporated into the model of a nonfailing myocyte for maintaining the resting level of $[Na^+]_i$ (10 mmol/L in both cell groups). In a failing myocyte, Na^+ ion extrusion by I_{NaK} balances the Na^+ ion entry by I_{NaCa} so that incorporation of $I_{Na,b}$ into this model is not necessary in that cell.

The model is written in Pascal and tested using a Turbo-Pascal compiler (Borland International) on an IBM-compatible computer with an Intel Pentium central processing unit. A fourth-order Runge-Kutta method with fixed time intervals is used for numerical integration of differential equations.

For the simulations in the present study, the fixed time interval for voltage-clamp simulations is 0.01 to 0.1 ms. The time interval for AP simulations is held at 0.0001 ms during the stimulus current and then set at 0.01 to 0.1 ms. APs are elicited in all simulations with 10

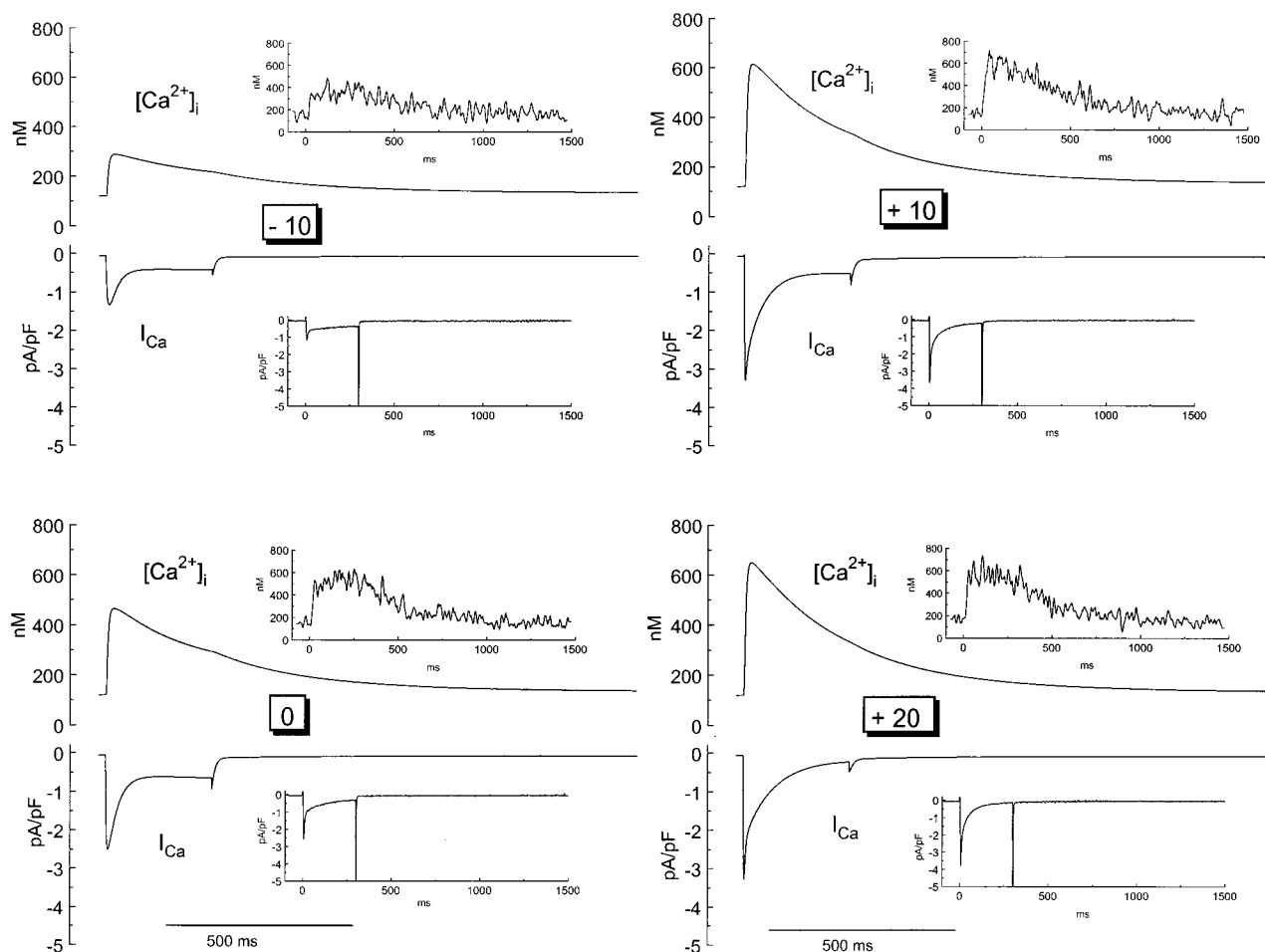


Figure 2. Ca^{2+} current through I_{Ca} and intracellular $[\text{Ca}^{2+}]_i$ of a nonfailing myocyte at various depolarizations in the model and in the experiment²⁷ (insets). Holding potential was -40 mV. As in the experimental study, I_{NaCa} was present in these simulations. $[\text{Na}^+]_i$ was 5 mmol/L.

pA/pF of I_{st} for 0.7 ms. Standard software is used to convert the simulated data in ASCII format and to prepare the figures. Fitting of the voltage-clamp traces is performed with a commercial software using a nonlinear least-squares algorithm.

Results

Simulations of Voltage-Clamp Experiments

An important test for the validity of an AP model is the accurate simulation of voltage-clamp experiments. Therefore, we have simulated the ionic currents I_{Ca} , I_{to} , I_{Kr} , I_{Ks} , and I_{K1} under voltage-clamp conditions using pulse protocols similar to those used in the experiments previously performed by our group^{13,27} and by Li et al.²¹ Figures 2 and 3 show I_{Ca} and $[\text{Ca}^{2+}]_i$ transients in a nonfailing and a failing myocyte, respectively. Experimental data are shown as insets. Simulations of $[\text{Ca}^{2+}]_i$ transients at various depolarizations were started with $[\text{Ca}^{2+}]_{\text{NSR}} = [\text{Ca}^{2+}]_{\text{JSR}} = 2.5$ mmol/L in a nonfailing myocyte and $[\text{Ca}^{2+}]_{\text{NSR}} = [\text{Ca}^{2+}]_{\text{JSR}} = 1.0$ mmol/L in a failing myocyte on the basis of experimental data.⁴⁹ Under these conditions, simulated and experimentally found I_{Ca} and $[\text{Ca}^{2+}]_i$ transients were similar in both cell groups. In particular, peak $[\text{Ca}^{2+}]_i$ was maximal when I_{Ca} reached its maximum at $+10$ mV in both cell groups. Values of resting and peak $[\text{Ca}^{2+}]_i$ (Table 2) at $+10$ mV are in the range of

experimental data.²⁷ Although peak I_{Ca} was slightly greater in a failing than in a nonfailing myocyte, the triggered $[\text{Ca}^{2+}]_i$ transient was smaller than in a nonfailing myocyte because of the lower Ca^{2+} content of the SR.

Figure 4 shows I_{to} simulated in a failing myocyte. The corresponding experimental traces are depicted in Figure 4B. The pulse protocol is shown as an inset. The current density of I_{to} at $+40$ mV (difference between peak current and maintained current at the end of the pulse) was 8.9 pA/pF. The time course of inactivation of I_{to} was largely independent of voltage. The time constant of its monoexponential decay in the voltage range of $+10$ to $+80$ mV was 13 ± 0.9 ms. These values of I_{to} are in accordance with experimental data measured at 37°C .²⁰ Figures 2, 3, and 4 demonstrate that simulated I_{Ca} , $[\text{Ca}^{2+}]_i$ transients, and I_{to} resemble the experimental recordings closely with regard to their magnitude and kinetics.

The simulations of voltage-clamp experiments of I_{Kr} and I_{Ks} are depicted in Figure 5. Depolarizations from a holding potential of -60 mV to the various clamp pulse potentials generate a rapidly activating (Figure 5A) and a slowly activating (Figure 5B) K^+ current through delayed rectifier channels with close approximation to experimental data.²¹ To validate simulations of I_{Kr} and I_{Ks} , current-voltage relations for I_{Ktail} of I_{Kr} and I_{Ks} are shown in Figure 5C. The values are

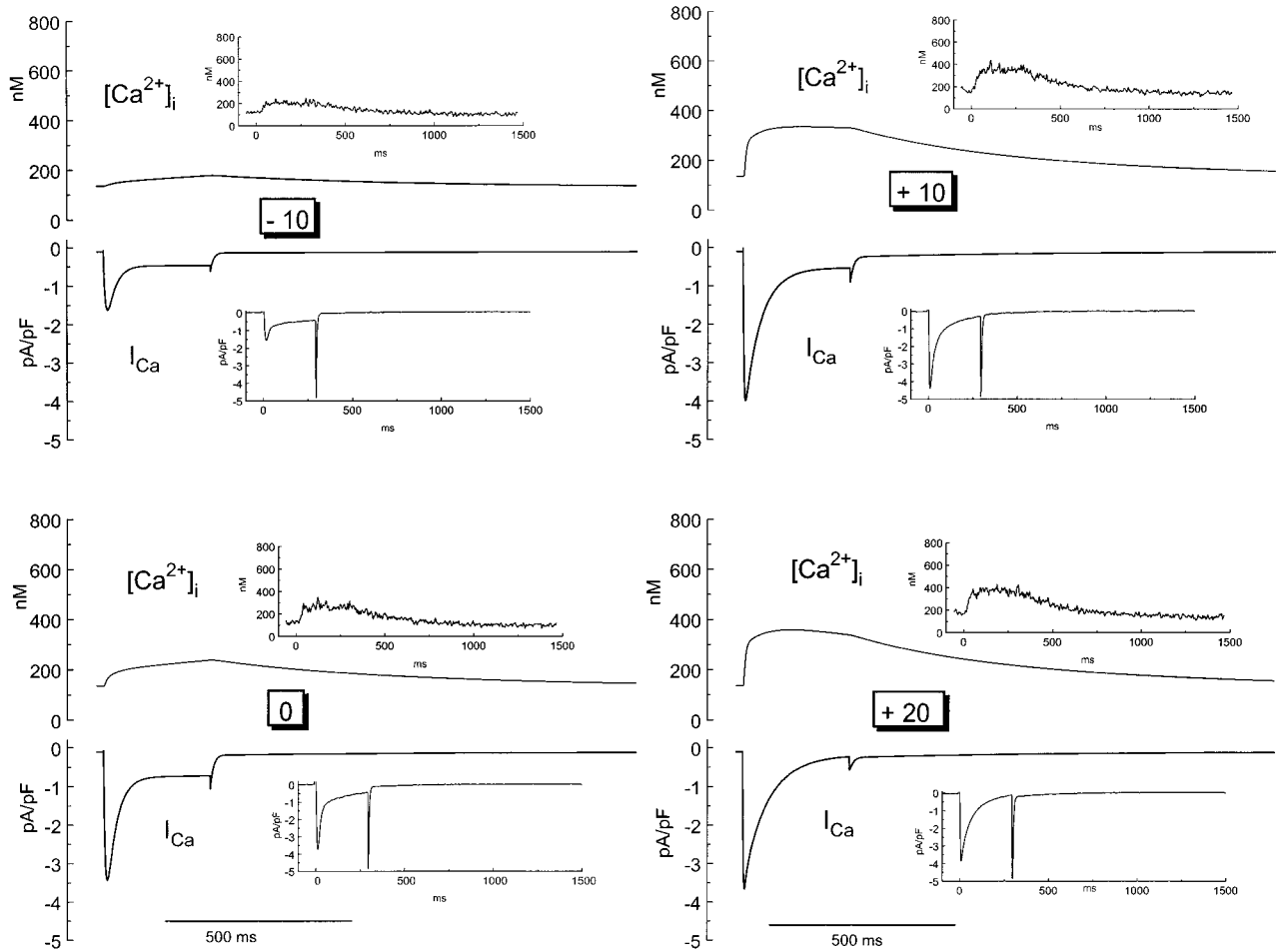


Figure 3. Ca^{2+} current through L-type Ca^{2+} channels (I_{Ca}) and intracellular $[\text{Ca}^{2+}]_i$ transients ($[\text{Ca}^{2+}]_i$) of a failing myocyte at various depolarizations in the model and in the experiment²⁷ (insets). Holding potential was -40 mV. As in the experimental study, I_{NaCa} was present in these simulations. $[\text{Na}^+]_i$ was 5 mmol/L.

very close to experimental data.²¹ Activation voltage dependence was determined by normalizing I_{Ktail} at each test potential in Figure 5C to the current at the most positive potential. Results are shown in Figure 5D. Curves are fitted to a Boltzmann distribution function. $V_{0.5}$ and k values are consistent with experimental results (Table 3).

Data of I_{K1} are shown in Figure 6. Experimental traces of I_{K1} in failing myocytes are depicted in Figure 6A. Currents were elicited from a holding potential of -30 mV to the indicated voltages. On the basis of these experimental data, I_{K1} was simulated using the same pulse protocol. The current-voltage relations of simulated I_{K1} in a nonfailing and a failing myocyte are shown in Figure 6B. The whole-cell current slope conductance at the reversal potential of I_{K1} in a failing myocyte is smaller (0.23 nS/pF) than that in a nonfailing myocyte (0.4 nS/pF). In addition, the current density of I_{K1} at -70 mV (0.6 pA/pF [failing myocyte] versus 0.8 pA/pF [nonfailing myocyte]) and at -100 mV (-10 pA/pF [failing myocyte] versus -15 pA/pF [nonfailing myocyte]) is assumed to be smaller in a failing than in a nonfailing myocyte.

Simulated AP Is Prolonged in Heart Failure

After showing that simulated ionic currents and $[\text{Ca}^{2+}]_i$ transients resemble experimental measurements, APs of a

nonfailing and of a failing myocyte were simulated. To obtain a steady state in $[\text{Ca}^{2+}]_i$ transients, 10 APs were elicited at a frequency of 1 Hz. Under these conditions, both APs are distinctly different (Figure 7, top; nonfailing, dashed line; failing, solid line).

APD_{90} was significantly longer in a failing than in a nonfailing myocyte (548.8 versus 374.0 ms, respectively). In contrast to this, differences in APD_{25} and APD_{50} between both cell groups were smaller (APD_{25} : nonfailing, 262.9 ms; failing, 305.7 ms; APD_{50} : nonfailing, 310.2 ms; failing, 374.5 ms). Therefore, the prolongation of APD in heart failure was mainly due to the slower rate of repolarization in the late phase of AP in a failing compared with a nonfailing myocyte, which was also found in an experimental study on human myocardium.⁵⁰ The ionic currents and the $[\text{Ca}^{2+}]_i$ transients

TABLE 2. $[\text{Ca}^{2+}]_i$ Regulation (Experimental Data and Model)

	Nonfailing		Failing	
	Resting, nmol/L	Peak, nmol/L	Resting, nmol/L	Peak, nmol/L
Beuckelmann et al ²⁷	96 ± 47	746 ± 249	165 ± 61	367 ± 109
Model	120	614	136	334

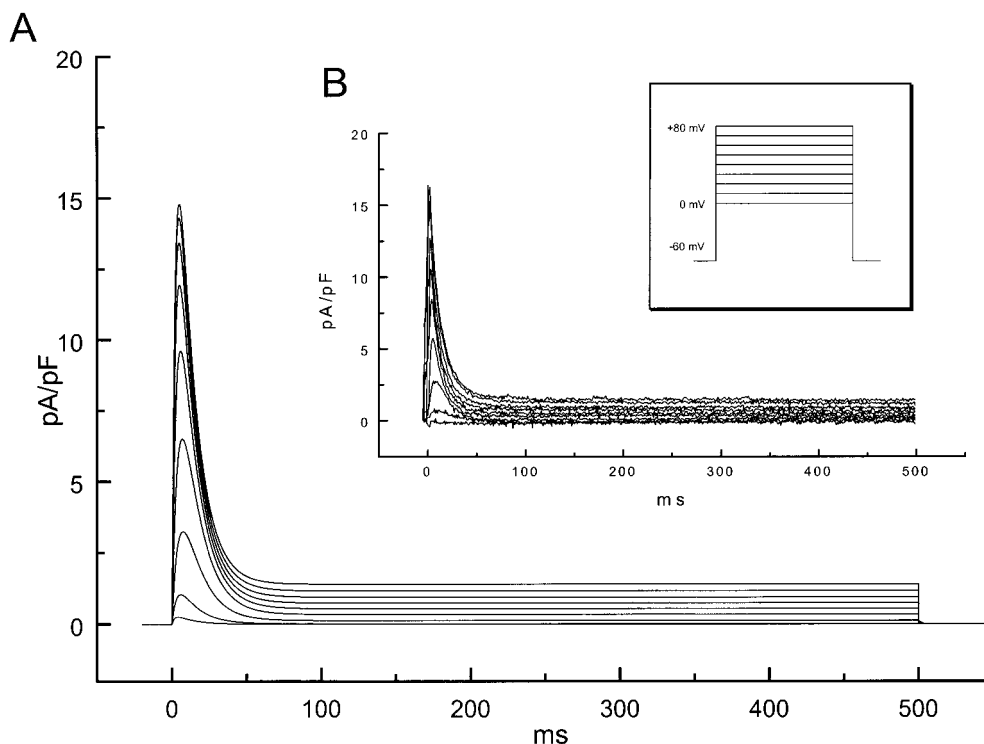


Figure 4. I_{to} of a failing myocyte in the model (A) and in the experiment (B). The pulse protocol is shown as an inset.

during the AP are shown in Figures 7 and 8 (nonfailing, dashed line; failing, solid line). At 4 mmol/L $[K^+]_o$ and 140 mmol/L $[K^+]_i$, the resting membrane potential in this model was only slightly different in both cell groups (non-failing, -89.7 mV; failing, -85.6 mV). A greater discrepancy in resting membrane potential between both cell groups was prevented by I_{K1} . Although the current density of I_{K1} was reduced in a failing compared with a nonfailing myocyte, the increase of I_{K1} in these cells when the resting potential becomes more positive limits the depolarization of the cell membrane in a failing myocyte (Figure 7, I_{K1}).

After depolarization of the cell membrane by a suprathreshold stimulus, I_{Na} depolarized the membrane to an overshoot potential of 50 mV and inactivated immediately (not shown). Subsequently, I_{Ca} , I_{to} , I_{Ks} , and I_{Kr} were activated, and I_{NaK} increased. The fast activation of I_{Ca} (5 ms) was followed by a rapid incomplete inactivation to 12% of its peak value (Figure 7). Repolarization was initiated by the activation of I_{to} . In both cell groups, I_{to} activated and inactivated rapidly (Figure 7). Thereafter, I_{Kr} and, subsequently, I_{Ks} were completely activated and accelerated the repolarization, which was completed by the opening of I_{K1} channels (Figure 7).

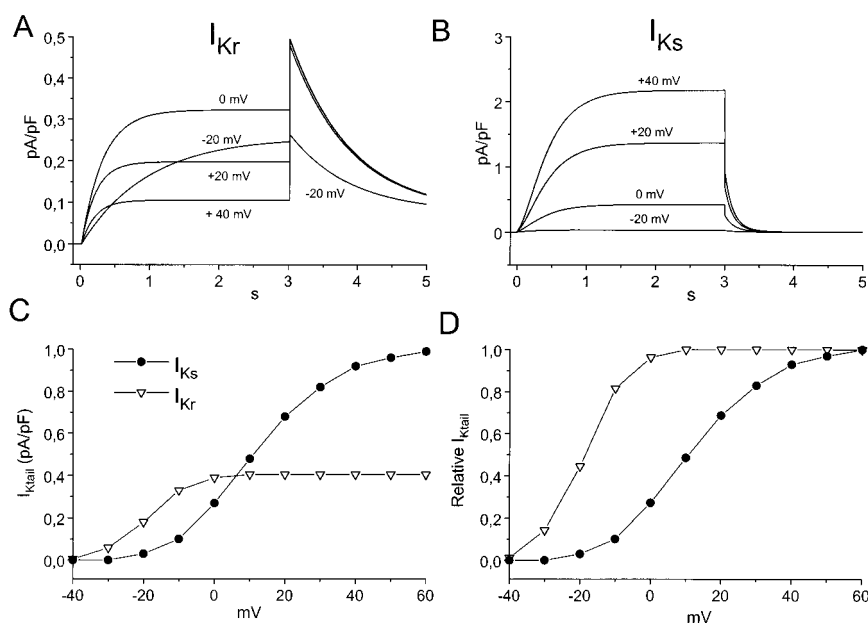


Figure 5. A and B, Simulation of the fast (I_{Kr} , A) and the slow (I_{Ks} , B) component of I_K based on the study by Li et al.²¹ Time-dependent step currents were elicited by depolarizations over 3 s to the indicated potentials from a holding potential of -60 mV. Tail currents were elicited by repolarizations to -30 mV over 2 s. Note the reduction of step current density of I_{Kr} at voltages negative to 0 mV. C, Current-voltage relations for I_{Ktail} of I_{Kr} (∇) and I_{Ks} (\bullet). I_{Ktail} was elicited by the same pulse protocol as described above. D, Activation curve of I_{Kr} and I_{Ks} based on analysis of I_{Ktail} in panel C.

TABLE 3. Parameters of Steady-State Activation of I_{Kr} and I_{Ks} (Experimental Data and Model)

Studies	I_{Ks}		I_{Kr}	
	$V_{0.5}$, mV	k , mV	$V_{0.5}$, mV	k , mV
Li et al ²¹	$+9.4 \pm 2.5$	$+11.8 \pm 2.9$	-14 ± 4	$+7.7 \pm 2.7$
Model	+10.6	+11.5	-18.9	+6.1

When these repolarizing currents increased, I_{Ca} deactivated completely. During the plateau and repolarization phase of AP, I_{NaK} counteracted the depolarization of the cell membrane (Figure 8).

The total current of the background currents, $I_{Ca,b}$ and $I_{Na,b}$, during an AP was slightly higher in a nonfailing myocyte (Figure 8), so that the alterations in APD in heart failure may even be underestimated.

In this model, I_{NaCa} was a repolarizing current during most of the AP plateau in a failing myocyte (Figure 7). During the late plateau and repolarization phase, I_{NaCa} carried an inward current in its forward mode and extruded Ca^{2+} ions out of the myocyte. By this means, I_{NaCa} becomes a depolarizing current. Therefore, it slows down the rate of membrane repolarization during the late phase of membrane repolarization, especially

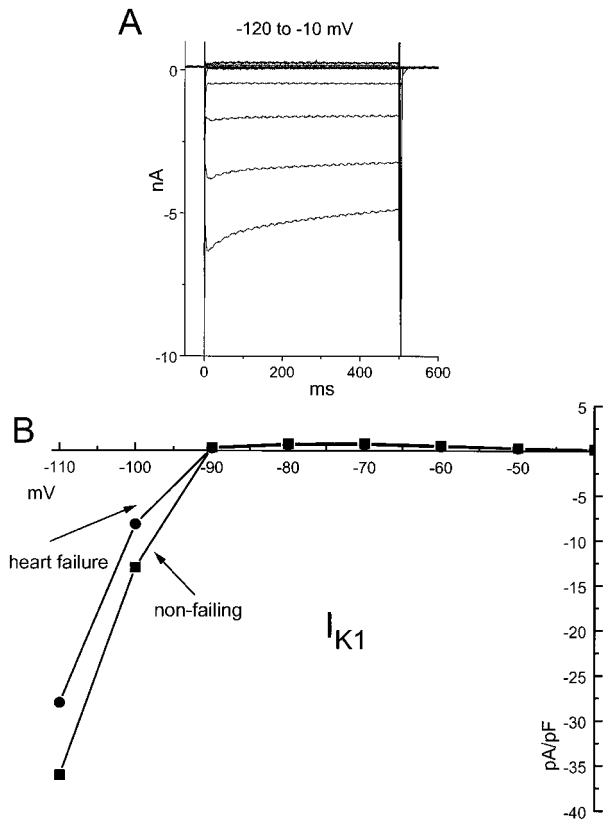


Figure 6. Inward rectifier current: I_{K1} . A, Original experimental recording from a holding potential of -30 mV. The cell was hyperpolarized to -120 to $+10$ mV over 500 ms. Note that the current was time dependent only on hyperpolarizations to potentials negative to -100 mV. B, Current-voltage relations of simulated I_{K1} in a nonfailing and a failing myocyte. Currents are simulated using the experimental pulse protocol as described above.

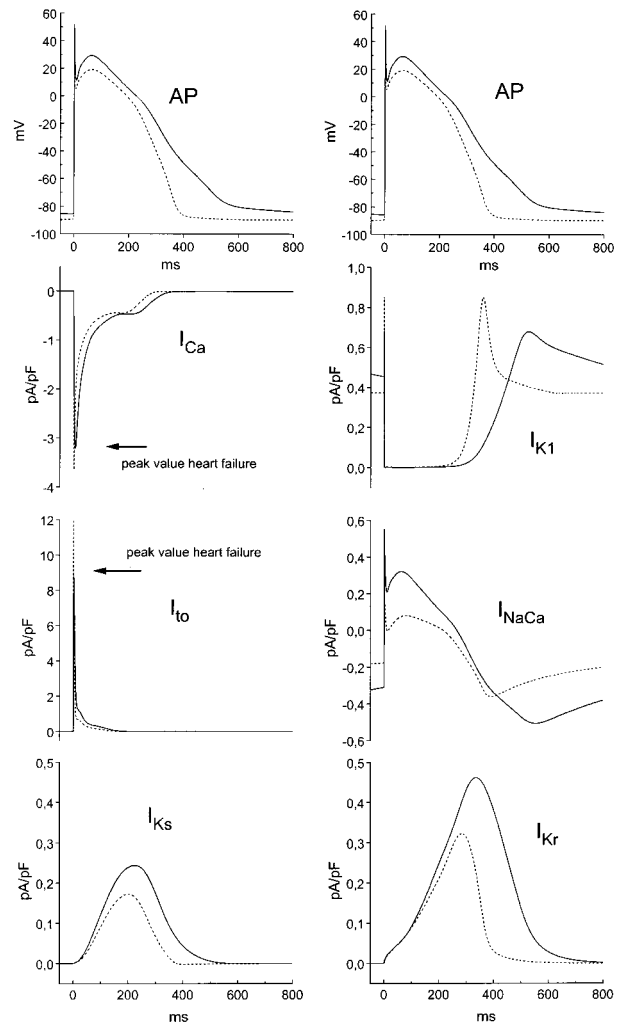


Figure 7. Simulated APs and major ionic currents determining the AP shape in a nonfailing myocyte (dashed line) and in a failing myocyte (solid line). For details, see text. Peak values of I_{Ca} and of I_{to} in a failing myocyte are indicated by arrows.

in a failing myocyte, because of its higher activity and the slowed decay of the $[Ca^{2+}]_i$ transient. In this myocyte, the final repolarization phase was also prolonged because of the decrease of I_{K1} (0.68 versus 0.85 pA/pF in a nonfailing myocyte) and of I_{NaK} .

The $[Ca^{2+}]_i$ transient during the AP was markedly different in both cell groups (Figure 8). As a result of the higher Ca^{2+} content in the SR, the maximum of the Ca^{2+} transient was higher in a nonfailing than in a failing myocyte (nonfailing, 1100 nmol/L; failing, 569 nmol/L). The faster inactivation of I_{Ca} in the nonfailing myocyte was caused by enhanced Ca^{2+} -dependent inactivation of this current and led, together with higher I_{to} and I_{NaK} , to a reduction of the plateau phase of the AP in this myocyte compared with a failing myocyte (nonfailing, +19.0 mV; failing, +29.2 mV).

In conclusion, these simulations of APs in both groups demonstrate that the prolongation of the AP in a failing myocyte is mainly due to a prolonged late repolarization phase caused by an enhanced activity of I_{NaCa} and the slowed diastolic decay of the $[Ca^{2+}]_i$ transient. The reduction of I_{K1}

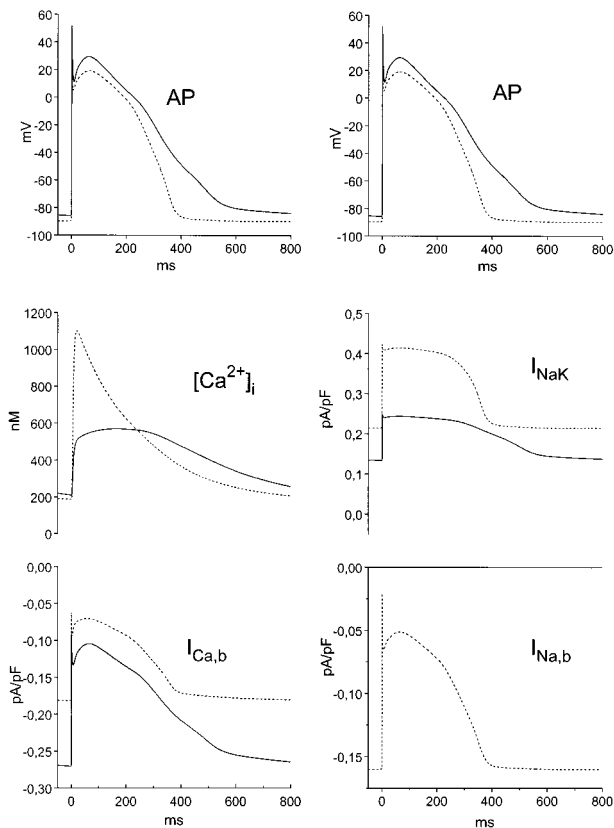


Figure 8. Simulations of the intracellular $[Ca^{2+}]_i$ transient ($[Ca^{2+}]_i$) in a nonfailing myocyte (dashed line) and in a failing myocyte (solid line) at a stimulation frequency of 1.0 Hz. In addition, I_{NaK} , $I_{Ca,b}$, and $I_{Na,b}$ are shown.

and I_{NaK} in heart failure additionally contribute to the difference in the late repolarization phase between nonfailing and failing myocytes.

Simulated APs Resemble Those Recorded in Human Ventricular Myocytes

APs in human ventricular myocytes of nonfailing and failing hearts measured in different laboratories show a great variability in duration and shape. Despite using comparable

isolation procedures and recording APs under maintained conditions, a significant variability remains. APs measured in our laboratory (Dr M. Lindner, unpublished data) vary more distinctly in failing than in nonfailing myocytes. Figure 9 shows measured APs that represent the observed spectrum. It is obvious that simulated APs (Figure 7) were generally similar to the measured APs in nonfailing (Figure 9A) and failing (Figures 9B and 9C) myocytes. However, a group of recorded APs in failing myocytes (Figure 9D) characterized by a pronounced prolonged plateau phase showed significant differences to the simulation. Possible underlying factors will be discussed later.

Simulated and Experimental APD Restitution Curves Are Similar

In the human heart, similar to other mammalian hearts, increasing the pacing rate or shortening of the coupling interval of a premature beat leads to shortening of the APD.^{51,52} The reconstruction of this physiological phenomenon by this model serves a very important purpose, ie, validation. Therefore, APD restitution was simulated according to the experimental protocol of Morgan et al.⁵¹ For this purpose, paired stimuli were used to elicit a second AP (AP2) at variable times after the initiation of the first (AP1). Before each simulation with a different time interval, 10 APs were elicited at a frequency of 1 Hz to obtain a steady state in $[Ca^{2+}]_i$ transients. For clarity, only APs at the following extrastimulus intervals are shown: 300, 400, 500, 600, 700, and 800 ms (Figure 10A). APD restitution curves are depicted in Figure 10B.

APD₉₀ of the second AP obtained in simulations (Figure 10B, circle) and in the experiment (Figure 10B, square) are plotted as function of extrastimulus interval. The similarity of both curves substantiates the validity of this model.

The Effect of I_{to} on the APD in Human Myocardium Is Small

4-Aminopyridine is known to prolong the AP. From this result, it has been postulated that reduction of I_{to} may prolong the AP in cardiac myocytes.^{13,53,54} However, there are additional effects of 4-aminopyridine on other currents, especially

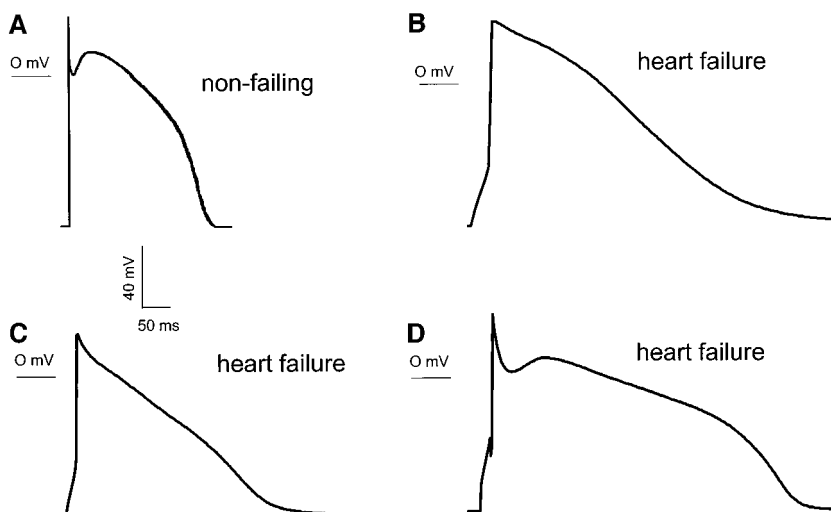


Figure 9. Measured APs in nonfailing (A) and failing (B to D) myocytes (M. Lindner, unpublished data). Note the great variability in shape and duration of APs in failing myocytes.

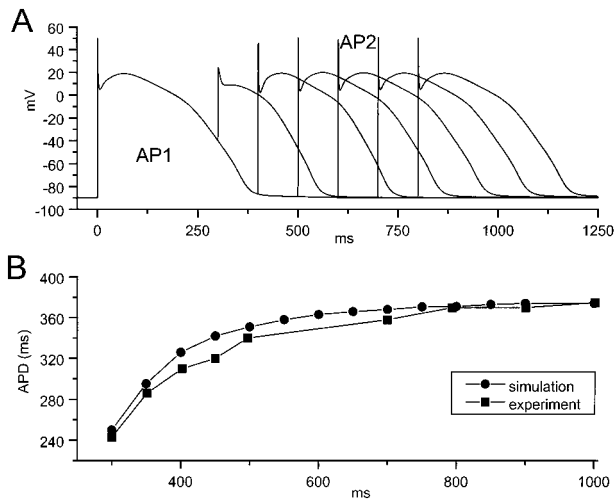


Figure 10. Restitution of APD. Simulations were performed in a nonfailing myocyte. A, The myocyte was initially paced 10 times at 1 Hz, and then an additional stimulus was applied, triggering a second AP (AP2) after variable intervals (IDs), defined as the time interval between the initiation of the last paced AP (AP1) and the upstroke of AP2. AP1 and AP2 are shown for 6 different IDs: 300, 400, 500, 600, 700, and 800 ms. B, APD₉₀ as function of ID is shown. Results of simulations (●) and experimental data (■) by Morgan et al⁵¹ are compared.

on I_{Ca}^{23} and I_{K}^{55} . With our model, we can investigate the possible contribution of I_{to} to the APD in human ventricular myocytes. To assess the effect of I_{to} on APD, we simulated the APs in both cell groups under conditions of various degrees of I_{to} inhibition (25%, 50%, 75%, and 100%). As described above, the simulations were preceded by 10 stimulations to obtain steady-state conditions. The simulated APs shown in Figure 11 demonstrate that inhibition of I_{to} does not significantly prolong the AP in a nonfailing (Figure 11A) or in a failing (Figure 11B) myocyte.

I_{Kr} and I_{Ks} Control Repolarization in Human Myocardium

Despite their relative small current densities, I_{Kr} and I_{Ks} largely control repolarization of the AP in human ventricular myocytes. This effect of I_{Kr} and I_{Ks} on APD in guinea pig ventricular myocytes has already been demonstrated in a previous computer simulation study.⁵⁶ Inhibition of I_{Kr} , the main mechanism of class III antiarrhythmic agents, has also been shown to prolong the AP in in vivo mapping studies.⁵⁷⁻⁵⁹

Carlsson et al⁶⁰ have found a pronounced prolongation of the AP in nonfailing human ventricular muscles after inhibition of I_{Kr} by 10^{-6} H 234/09 (almokalant). At this concentration, almokalant significantly blocks only I_{Kr} .⁶¹

We attempted to imitate this effect of I_{Kr} on APD in human myocardium by varying g_{max} of I_{Kr} to 75%, 50%, 25%, and 0% of its original value. To obtain a steady state of the $[Ca^{2+}]_i$ transient, 20 action potentials were elicited. Figure 12A shows the prolongation of the AP in a nonfailing cell by inhibition of I_{Kr} to various degrees (left). As in the experimental study,⁶⁰ increased inhibition of I_{Kr} resulted in a progressive prolongation of AP. At 100% inhibition of I_{Kr} , APD₉₀ was lengthened from 374.0 to 689.4 ms, which is in the range measured by Carlsson et al.⁶⁰ This APD prolonga-

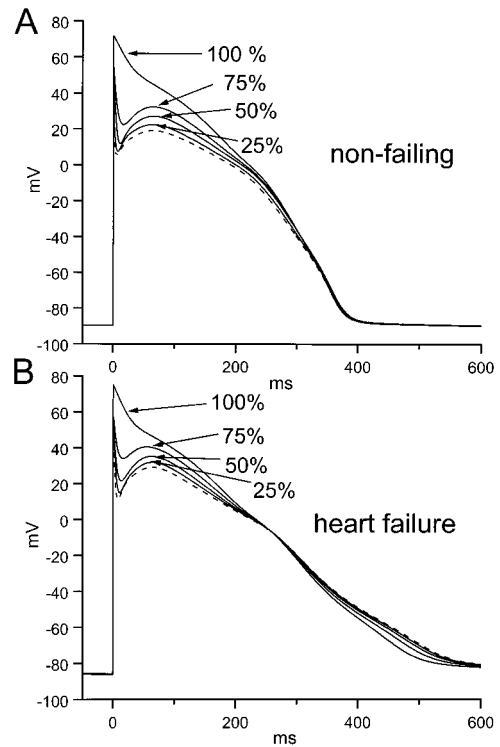


Figure 11. Effect of inhibition of I_{to} on the APD. APs were simulated at various degrees of inhibition of I_{to} in a nonfailing myocyte (A) and in a failing myocyte (B). These simulations imply that I_{to} has only a small effect on the APD in human myocardium.

tion was, however, larger than that found in single human myocytes after 100% inhibition of I_{Kr} by Li et al.²¹ This discrepancy may be partially due to the different experimental conditions. In contrast to our simulations, the intracellular Ca^{2+} was buffered by using 5 mmol/L EGTA, significantly influencing I_{Ca} and, thereby, the AP. Inhibition of I_{Kr} also prolonged AP in a failing myocyte (Figure 12B, left). In contrast to a nonfailing myocyte, 50% inhibition of I_{Kr} resulted in an incomplete repolarization of the cell membrane in a failing myocyte at 1.0 Hz (Figure 12B, left; 50%). At 75% inhibition of I_{Kr} , even an EAD developed after 3 stimulations. Therefore, a failing myocyte is more sensitive than a nonfailing myocyte to I_{Kr} inhibition. Simulations with various degrees of inhibition of I_{Ks} have indicated that this current also has a significant impact on APD in both cell groups (Figure 12A and 12B, right). However, inhibition of I_{Kr} had an even greater effect. In a nonfailing myocyte, 100% inhibition of I_{Ks} prolonged APD₉₀ from 374.0 to 526.1 ms. In a failing myocyte, incomplete repolarization occurred at 100% inhibition of I_{Ks} .

Complete Inhibition of I_{Kr} Induces Development of Recurrent EADs in Failing Myocytes

The previous simulations reveal the critical role of I_{Kr} in repolarization and, thereby, in the electric stability of the cell membrane in a failing myocyte. Therefore, inhibition of I_{Kr} may facilitate the formation of EADs in failing myocytes. At 75% inhibition of I_{Kr} , we can observe an EAD after 3 stimulations. To investigate whether there are recurrent EADs in a failing myocyte without preconditioning stimulations,

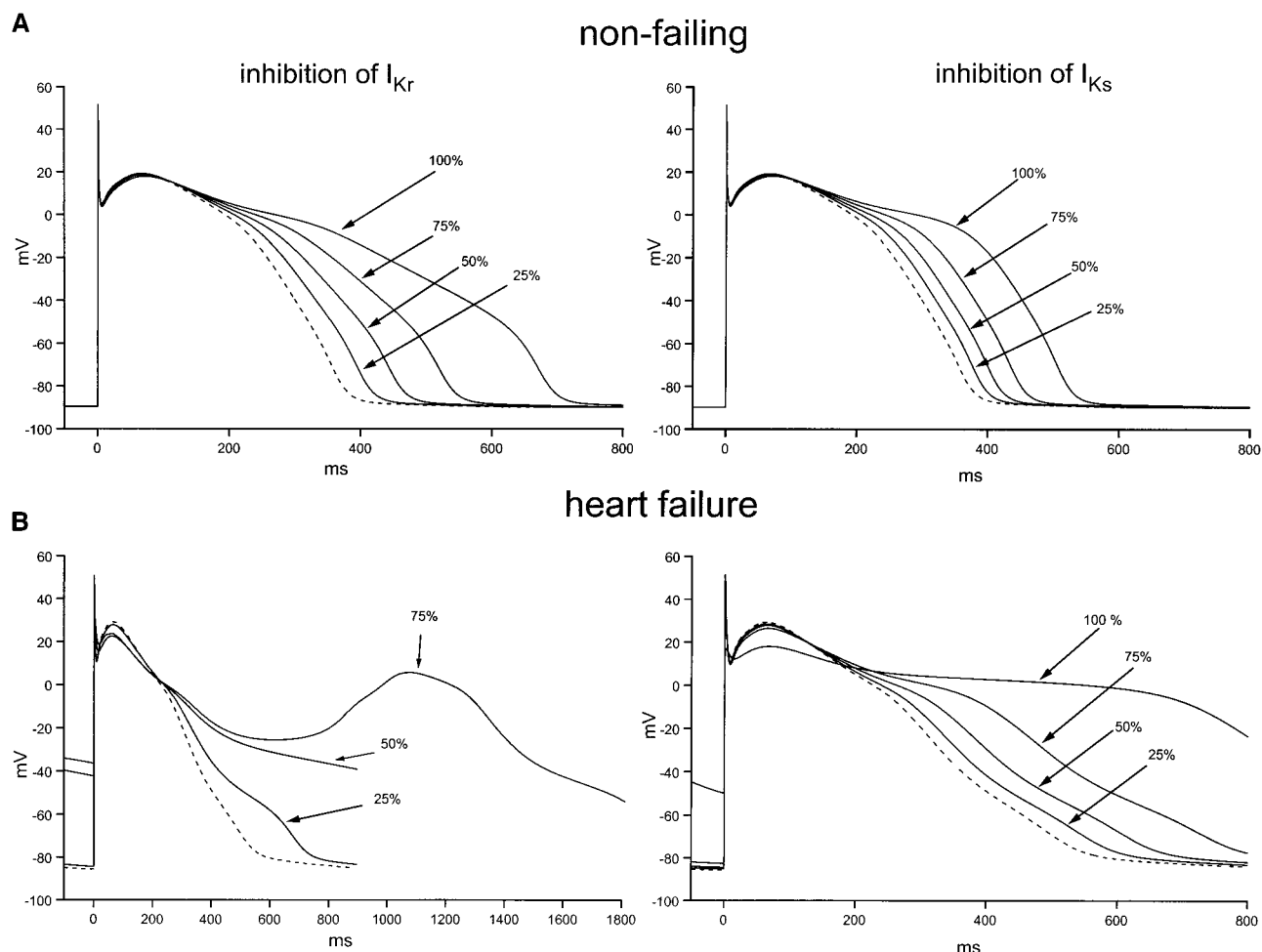


Figure 12. Simulated APs under control conditions (dashed line) and when g_{max} of I_{Kr} or I_{Ks} was reduced by 25%, 50%, 75%, or 100% in a nonfailing myocyte (A) and in a failing myocyte (B).

simulation of the action potential in a failing myocytes was performed while assuming complete inhibition of I_{Kr} . The computed AP, $[Ca^{2+}]_i$ transient, and I_{Ca} and I_{NaCa} are shown in Figure 13. It is obvious that 100% inhibition of I_{Kr} leads to recurrent EADs in a failing myocyte. I_{Kr} inhibition prolonged the time when the membrane potential was at ≈ -30 mV. This allowed for sufficient time for reactivation of I_{Ca} and for generation of EADs. During the decay phase of EADs, I_{NaCa} transiently becomes a depolarizing current. However, the magnitude of I_{NaCa} (-0.05 pA/pF) was much smaller than that of I_{Ca} (-0.5 pA/pF). Therefore, it can be concluded that EADs are mainly carried by I_{Ca} in our model.

The Likelihood of Premature APs Is Enhanced in a Failing Myocyte

Premature APs can be triggered by DADs, which are caused by a spontaneous Ca^{2+} release from the SR.^{62,63} Since I_{NaCa} as a possible underlying current is enhanced in failing myocytes, it can be expected that premature APs occur more frequently in these myocytes than in nonfailing cells. However, there is evidence that the Ca^{2+} content of SR is decreased in failing myocytes, which would lead to a smaller Ca^{2+} increase after spontaneous Ca^{2+} release from the SR and, thereby, to a reduced driving force for the depolarizing I_{NaCa} in these cells.

Therefore, it remains unclear whether increased I_{NaCa} in failing myocytes is indeed combined with a higher occurrence of DADs. Additionally, it should be pointed out that DADs are not, per se, arrhythmogenic. One could rather imagine that the generation of DADs would result in reduced excitability of the myocyte by affecting the availability of Na^+ channels. The generation of DADs exerts a solely proarrhythmic effect if the depolarization reaches the threshold to open Na^+ channels and trigger a premature AP. Consequently, we investigated whether the combined electrophysiological alterations in heart failure would enhance the likelihood of premature APs. For this purpose, a spontaneous Ca^{2+} release from the SR was simulated in both cell groups. As Luo and Rudy⁶⁴ have shown, the recovery from the slow inactivation of Na^+ channels, named factor j in their model, determines the recovery of the excitability after the AP. To investigate the influence of I_{NaCa} on the generation of premature APs separately, the Na^+ channels should be completely recovered from their slow inactivation at the start of the spontaneous Ca^{2+} release from the SR. Therefore, a spontaneous Ca^{2+} release from SR was assumed to occur at least 250 ms after 90% repolarization of the last AP in both cell groups. After this diastolic time interval, the factor $j=1$ (eg, the availability of Na^+ channels) was $\approx 100\%$ in both cell groups.

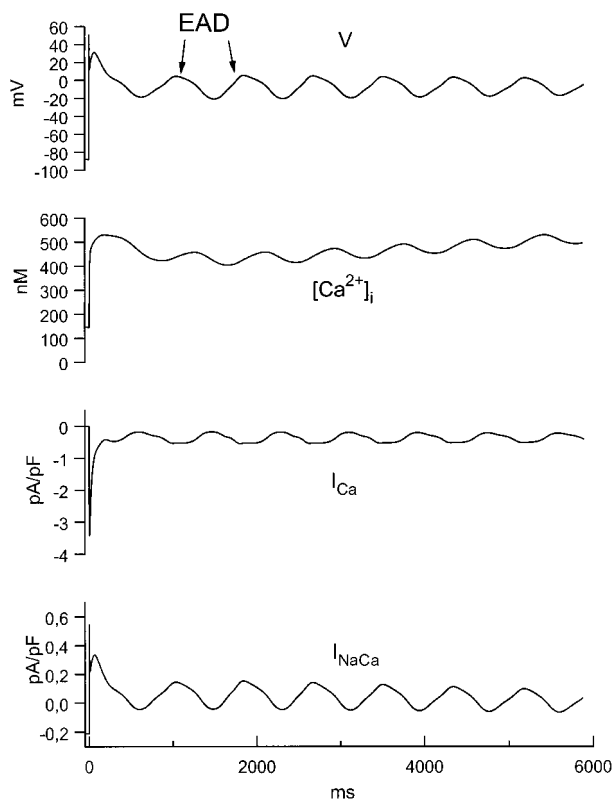


Figure 13. Generation of recurrent EADs in a failing myocyte after complete inhibition of I_{Kr} . V indicates membrane potential.

We assumed an equal Ca^{2+} -independent mechanism of the spontaneous Ca^{2+} release from the SR in both cell groups. Simulations of spontaneous Ca^{2+} release from the SR were preceded by a train of stimulations at 2.0 Hz for elevating the Ca^{2+} content of the SR. After 11 stimulations, there were differences in Ca^{2+} homeostasis between both cell groups (Figures 14 and 15). Before spontaneous Ca^{2+} release occurred, diastolic $[Ca^{2+}]_i$ was higher in a failing myocyte (275 nmol/L) than in a nonfailing myocyte (218 nmol/L). $[Ca^{2+}]_{NSR}$ was increased from 2.9 to 3.4 mmol/L in a nonfailing myocyte and from 1.2 to 1.5 mmol/L in a failing myocyte. As expected, the postulated spontaneous Ca^{2+} release from the SR resulted in a greater increase of $[Ca^{2+}]_i$ in a nonfailing myocyte (1394 nmol/L) than in a failing myocyte (713 nmol/L).

As a result, depolarizing peak I_{NaCa} was greater in a nonfailing than in a failing myocyte (-1.35 versus -1.0 pA/pF, respectively), although the activity of the Na^+ - Ca^{2+} exchanger was elevated in the failing myocyte. However, a premature AP was generated only in a failing myocyte (Figure 15).

Discussion

General Findings

Results of simulations of ionic currents and of the APD restitution show that this model can reproduce important electrophysiological characteristics of human ventricular myocytes. Voltage-clamp simulations of the major ionic currents (Figures 2 to 6) and the simulation of AP (Figure 7)

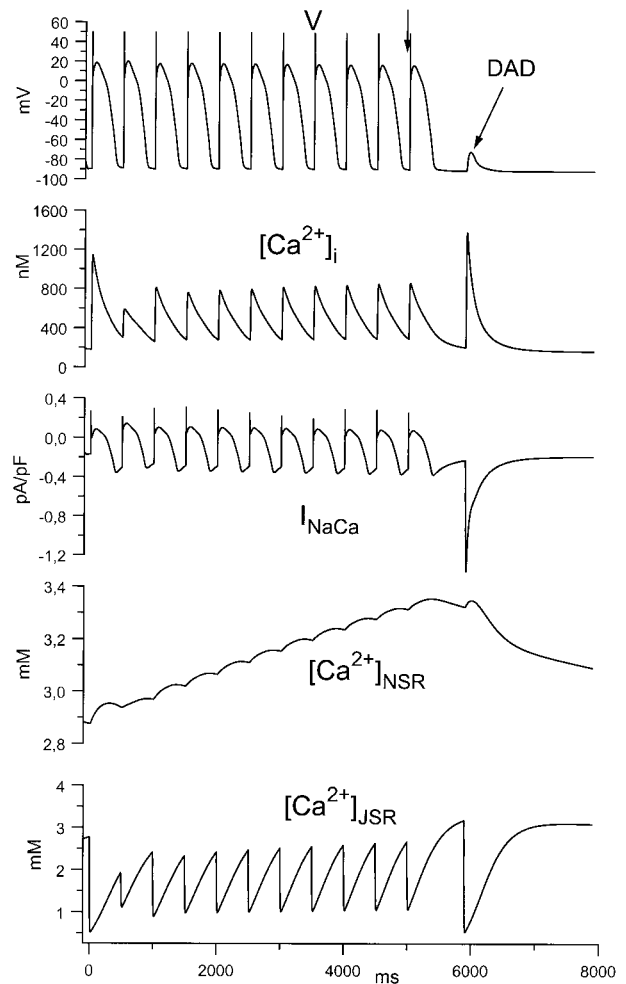


Figure 14. Effect of spontaneous Ca^{2+} release from the SR in a nonfailing myocyte. V indicates membrane potential. To enhanced Ca^{2+} content concentration of the NSR and JSR ($[Ca^{2+}]_{NSR}$ and $[Ca^{2+}]_{JSR}$), 11 APs were elicited at a frequency of 2.0 Hz. Spontaneous Ca^{2+} release from the SR was assumed to happen 250 ms after the last AP (indicated by an arrow). Subsequently, $[Ca^{2+}]_i$ increased quickly to a maximum level of 1394 nmol/L and then declined. This is linked to the generation of a DAD through a depolarizing I_{NaCa} .

closely resemble experimental data obtained from human single myocytes. Simulations of the ionic currents during the time course of the action potential (Figures 7 and 8) and simulations of ionic current inhibition reveal the important role of I_{Kr} and I_{Ks} in repolarization in human ventricular myocytes. I_{NaK} may additionally contribute to repolarization in human ventricular myocytes and, together with I_{K1} , stabilize the resting potential (Figure 8). Furthermore, simulations of ionic currents during the AP demonstrate that I_{NaCa} is an important depolarizing current during the late phase of repolarization in a failing myocyte (Figure 7) because of the enhanced activity of the Na^+ - Ca^{2+} exchanger and the slow decay of the $[Ca^{2+}]_i$ transient in this cell (Figure 8). In contrast to the results from an AP model of guinea pig ventricular myocytes,⁵⁶ we have found that the influence of I_{Kr} on APD is greater than that of I_{Ks} . This discrepancy is due to a much smaller ratio of g_{max} of I_{Ks} to I_{Kr} in the present study (1.3) compared with the animal model (7.72). Our value is

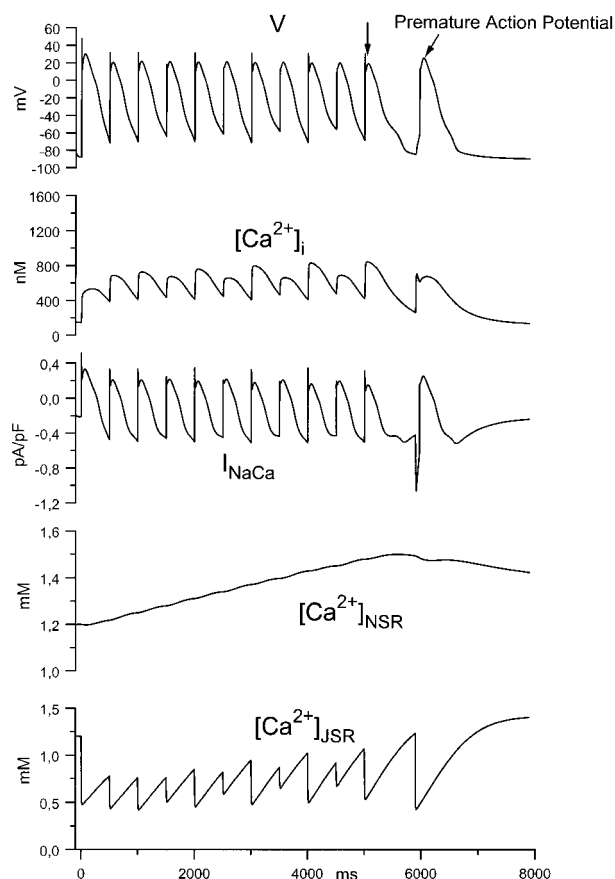


Figure 15. Effect of spontaneous Ca^{2+} release from the SR in a failing myocyte. V indicates membrane potential. As in a nonfailing myocyte, 11 APs were elicited at a frequency of 2.0 Hz to enhanced Ca^{2+} content concentration of NSR and JSR ($[\text{Ca}^{2+}]_{\text{NSR}}$ and $[\text{Ca}^{2+}]_{\text{JSR}}$). However, the increase was smaller compared with a nonfailing myocyte. Spontaneous Ca^{2+} release from the SR was assumed to happen 250 ms after the last AP (indicated by an arrow). In contrast to a nonfailing myocyte, $[\text{Ca}^{2+}]_i$ increased only to a maximum level of 713 nmol/L. This results, however, in a premature AP.

validated by simulations of current-voltage relations of tail currents of I_{Kr} and I_{Ks} , which are very close approximations to experimental data (Figure 5C). Although the g_{max} of I_{Ks} is still greater than that of I_{Kr} in the present study, I_{Ks} contributes a smaller fraction of the total I_{K} during a ventricular AP because of its slow activation kinetics (Figure 5B).

The influence of I_{Kr} and I_{Ks} on APD may be one reason for the wide range of measured APDs in different publications (between 233 ms¹⁷ and 650 ms¹³ in single myocytes from nonfailing hearts). Yue et al⁶⁵ have demonstrated that the expression of I_{K} in cells isolated from the canine heart is very dependent on the isolation technique.

Among other factors, different expressions of I_{Kr} and I_{Ks} in single human myocytes, possibly due to different isolation procedures, could be a reason for this divergence of APD. However, the AP simulated in a nonfailing myocyte (Figure 7) in our model very closely resembles the AP measured in single cells by our work group (Figure 9A) and by Peeters et al.⁵⁹ When the monophasic AP technique was used in in vivo studies,^{51,52} the observed shape and duration of AP in human hearts were very similar to our simulations.

In studies of various animal models of heart failure or hypertrophy, a reduction of I_{to} has been found, and this has been assumed to be an important factor causing AP prolongation in heart failure.^{54,66,67} In human ventricular myocytes, inhibition of I_{to} has been found to prolong AP.¹³ Our simulations of different degrees of inhibition of I_{to} (Figure 10) suggest, however, that inhibition of I_{to} does not prolong AP in nonfailing or failing myocytes in human hearts. A reason for this discrepancy could be that 4-aminopyridine, which was used in the experimental study,¹³ also blocked I_{Ks} and I_{Kr} , which would lengthen the AP. Considering this problem in experimental conditions, we conclude from the simulations of our model that the influence of I_{to} on APD is negligible in human myocardium. Of course, this model cannot prove that I_{to} does not alter APD, but it strongly suggests that reduction of the current density of I_{to} found in failing myocytes of human hearts does not seem to contribute significantly to the APD prolongation in heart failure. This hypothesis should be tested experimentally using a highly specific blocker of I_{to} in the future. In a human atrial AP model, it has been demonstrated that the effect of I_{to} on the AP is largely dependent on the magnitude of I_{K} .⁶⁸

Therefore, the distinctly different influence of I_{to} on APD in human ventricular myocytes compared with other cell types and species may be caused mainly by the specific kinetics and magnitude of I_{Kr} and I_{Ks} found in human ventricular myocytes. In myocytes, where I_{K} is found to be small, I_{to} may significantly determine the repolarization phase of the AP.⁶⁹

Prolongation of the AP in human ventricular myocytes of failing hearts has been well established.^{13,22,24,26} Most authors have found the APD to range between 400 and 1260 ms. In most of these studies, intracellular Ca^{2+} was buffered using EGTA in the pipette solution. Therefore, the influence of I_{NaCa} on the prolongation of the AP can be only slight in these studies. Our simulations suggest that an APD of >600 ms can be explained only by assuming a significant reduction of I_{Kr} or I_{Ks} (Figure 12). In those studies in which APD was very long, the authors could indeed detect only a small I_{Kr} and no I_{Ks} .^{13,24} As in nonfailing myocytes, the variability in shape and duration of APs in failing myocytes measured in our laboratory and in others could possibly be explained by a variable expression of I_{Kr} and I_{Ks} (Figure 9B to 9D). Further studies are necessary to show whether alterations of I_{Kr} and I_{Ks} in failing myocytes reflect real current changes in heart failure or whether they are caused by the isolation procedure.

Conclusions From the Simulated APs for Arrhythmogenesis in Heart Failure

From the results shown in Figures 14 and 15, we conclude that in heart failure one important mechanism for triggered arrhythmias could be DADs. In our model, DADs were initiated by a postulated spontaneous Ca^{2+} release from the SR. The resulting $[\text{Ca}^{2+}]_i$ increase depolarized the cell membrane through I_{NaCa} in both cell groups. Therefore, as in animal myocytes, this indicates that I_{NaCa} may also significantly contribute to the generation of DADs in human myocytes.

Although the activity of the Na^+ - Ca^{2+} exchanger is enhanced in failing myocytes, I_{NaCa} is slightly larger in nonfailing than in failing myocytes, since the $[\text{Ca}^{2+}]_i$ increase is much higher in this cell. Nevertheless, a premature AP can be triggered only in a failing myocyte as the repolarizing ionic currents, I_{K1} and I_{NaK} , are reduced in this cell. This indicates that a reduction of repolarizing currents (I_{K1} and I_{NaK}) rather than an increase of the depolarizing current (I_{NaCa}) seems to be responsible for the enhanced likelihood of triggered APs in failing myocytes. In our model, the increase of the Na^+ - Ca^{2+} exchanger activity in a failing myocyte can only partially compensate the smaller $[\text{Ca}^{2+}]_i$ increase as a driving force after spontaneous Ca^{2+} release from the SR. It should be pointed out that the conclusion of these simulations is limited by the assumption that the spontaneous Ca^{2+} release from the SR is self-initiated and equal in both cell groups. This limitation is necessary because our understanding of the mechanisms involved in the spontaneous Ca^{2+} release from the SR is incomplete. At present, the mechanism of the spontaneous Ca^{2+} release from the SR is thought to be a Ca^{2+} overload of the cell.^{70,71} Since the Ca^{2+} content of the SR increases faster in a nonfailing than in a failing myocyte at 2.0 Hz (Figures 14 and 15), the spontaneous Ca^{2+} release from the SR after pacing burst and resulting DADs is expected to occur earlier and more frequently in a nonfailing than in a failing myocyte, assuming that spontaneous Ca^{2+} release occurs if the Ca^{2+} content of the SR reaches a threshold level. This is, however, in contrast to experimental animal studies in which DADs and triggered APs were observed more frequently in failing or hypertrophied animal myocytes.^{72,73} The development of this model is inadequate to resolve this discrepancy. It cannot predict the occurrence of spontaneous Ca^{2+} release from the SR in both cell groups. Nevertheless, it may help to elucidate whether there are differences in the induction of DAD-triggered APs between both cell groups. Indeed, the simulations clearly show that spontaneous Ca^{2+} release leads to a triggered AP only in a failing myocyte. From these triggered APs, triggered arrhythmias may arise.

Even if we assume a higher incidence of spontaneous Ca^{2+} release from the SR in nonfailing myocytes, the higher incidence of resulting DADs would not result in a higher incidence of triggered arrhythmias than in failing myocytes.

The conclusion about the role of I_{NaCa} in DADs and triggered APs does not mean that the Ca^{2+} -dependent non-specific cation channel has no role in the arrhythmogenesis in heart failure. In animal studies, there is evidence for its contribution in generating DADs.^{74,75} Luo and Rudy⁷⁶ concluded from the results of their simulations that the contribution of $I_{\text{ns(Ca)}}$ and I_{NaCa} to the induction of DADs depends on the level of Ca^{2+} overload. However, at present, the existence of a nonspecific cation channel in human ventricular myocardium is unknown.

EADs are triggered during the plateau phase of an AP and are thought to be caused by reactivation of the I_{Ca} .^{6,7} The membrane potential has to remain at voltages positive to -35 mV until the L-type Ca^{2+} channels are able to recover from their inactivation and can open again. Detailed models have been developed addressing this issue. Nordin and Ming⁷⁷ showed that current-induced EADs in guinea pig ventricular

myocytes are mainly due to the L-type Ca^{2+} channel window current. Zeng and Rudy⁷⁸ came to the same conclusion in their model simulating the effect of cesium, Bay K 8644, and isoproterenol on the AP. In various preparations, specific block of I_{Kr} has been found to result in EADs in nonfailing animal myocytes. However, EADs are not generated by inhibition of I_{Kr} block in a nonfailing myocyte in this model (Figure 12A, left). Even if the g_{max} of I_{Kr} and I_{Ks} is changed simultaneously, corresponding to the approach of Zeng et al⁵⁶ to generate EADs in their model, no EADs can be generated in a nonfailing myocyte (not shown). In contrast to this, 75% inhibition of I_{Kr} can lead to an EAD in a failing myocyte (Figure 12B, left; 75%). When the inhibition of I_{Kr} is 100%, even recurrent EADs develop in this myocyte (Figure 13).

As already demonstrated in previous models,^{77,78} reactivated I_{Ca} is also the underlying inward current of these EADs. In conclusion, our results indicate that EADs are difficult to induce in human compared with animal myocytes. They can be generated only in failing myocytes after blocking I_{Kr} by at least 75% (Figure 12B, left, and Figure 13). This discrepancy in EAD formations between animal models and the present model is supported by experimental data. Vermeulen et al⁷³ have observed that EADs occur only in papillary muscles of rabbit hearts but never in human papillary muscles. Further studies are required to assess the role of EADs in arrhythmias in human ventricular myocytes.

Besides triggered APs, reentry mechanisms may also contribute to the increased incidence of tachyarrhythmias in heart failure.⁷⁹ Among many promoting factors, dispersion of refractoriness or wide variations in the duration of APs observed in hypertrophied myocardium⁸⁰ can evoke reentry arrhythmias.⁸¹ Our model can also contribute to the investigation of this type of arrhythmia in heart failure by identifying the ionic currents that are important for the APD in human ventricular myocytes. The simulations demonstrate that I_{Ks} has an impact on AP in the human heart. Regional differences of I_{Ks} reported in canine left ventricle⁸² could partially explain the known heterogeneity of the AP in human left ventricle.⁸³ This may also hold true to an increased extent in heart failure. In addition, the increase of I_{NaCa} activity and the alterations of $[\text{Ca}^{2+}]_i$ handling may also not be uniform in heart failure, thereby increasing the inhomogeneity of the AP across the heart wall. Another factor determining dispersion of APs along the myocardial wall could be the passive electrical properties of the myocardium. Keung et al⁸⁴ have demonstrated that these are different in normal and hypertrophied rat myocardium. Further studies are necessary to determine whether it also holds true in the human heart.

Limitations of the Model

A variety of models have been developed previously on the basis of the results of animal studies.^{31,56,85–88} Since major differences exist in the characteristics of ionic currents between human and animal myocytes, conclusions drawn from these models cannot easily be extrapolated to human heart cells. However, although the present model has the advantage of being based partially on human data, it also has several limitations.

Significant uncertainty remains concerning the magnitude of I_{NaCa} . At present, voltage-clamp data of this current in human ventricular myocytes are not available. Comparison of I_{NaCa} incorporated in the model with the measured data in the human atrium suggests that the magnitude of the simulated I_{NaCa} has been well estimated. Nevertheless, it should be pointed out that some results have to be interpreted with caution because of their dependence on I_{NaCa} . However, the simulations clarify that an increase of I_{NaCa} could play an important role in the arrhythmogenesis in heart failure and that its quantification in human ventricular myocytes is desirable.

To simulate $[Ca^{2+}]_i$ transients, the approach of the LR model is used. Although major components of intracellular Ca^{2+} homeostasis are included in this model, this approach is only an approximation of the complex nature of the intracellular Ca^{2+} homeostasis, since some important features, such as the CICR from the SR or the mechanism of Ca^{2+} buffering, and their potential changes in heart failure are simplified. This is mainly due to our incomplete understanding of the exact mechanisms involved in these phenomena. Nevertheless, the simulated $[Ca^{2+}]_i$ transients in both cell groups agree largely with experimental observations and provide an independent test of how well our model describes $[Ca^{2+}]_i$ homeostasis.

Another assumption of the model that has not been investigated is that I_{Kr} and I_{Ks} are unaltered in heart failure. In addition, information about I_{Kr} dependence on $[K^+]_o$ and I_{Ks} dependence on $[Ca^{2+}]_i$ is not available at present.

Therefore, it should be stressed that further development of this model is needed for simulating alterations of the APs under various pathophysiological conditions, such as myocardial ischemia, as performed by Shaw and Rudy.⁸⁹ Nevertheless, the conclusions from the simulations presented here, and also their limitations, highlight several important areas that deserve future experimental studies.

Appendix: Formulations of Ionic Currents

Inward Current

Fast Na^+ Current: I_{Na}

$$I_{Na} = 16 \cdot m^3 \cdot h \cdot j \cdot (V - E_{Na})$$

$$E_{Na} = (RT/F) \cdot \ln([Na^+]_o/[Na^+]_i)$$

where m , h , and j are the activation gate, the fast inactivation gate, and the slow inactivation gate of I_{Na} , respectively, V is the membrane potential, E_{Na} is the equilibrium potential for Na^+ , R is the universal gas constant, T is the absolute temperature, and F is the Faraday constant.

For $V \geq -40$ mV

$$\alpha_h = \alpha_j = 0.0$$

$$\beta_h = 1 / (0.13 \cdot \{1 + \exp[(V + 10.66) / -11.1]\})$$

$$\beta_j = 0.3 \cdot \exp(-2.535 \cdot 10^{-7} \cdot V) / \{1 + \exp[-0.1 \cdot (V + 32)]\}$$

For $V < -40$ mV

$$\alpha_h = 0.135 \cdot \exp[(80 + V) / -6.8]$$

$$\beta_h = 3.56 \cdot \exp(0.079 \cdot V) + 3.1 \cdot 10^5 \cdot \exp(0.35 \cdot V)$$

$$\alpha_f = [-1.2714 \cdot 10^5 \cdot \exp(0.244 \cdot V) - 3.474 \cdot 10^{-5} \cdot \exp(-0.04391 \cdot V)] \cdot (V + 37.78) / \{1 + \exp[0.311 \cdot (V + 79.23)]\}$$

$$\beta_f = 0.1212 \cdot \exp(-0.01052 \cdot V) / \{1 + \exp[-0.1378 \cdot (V + 40.14)]\}$$

For the total range of V

$$\alpha_m = 0.32 \cdot (V + 47.13) / \{1 - \exp[-0.1 \cdot (V + 47.13)]\}$$

$$\beta_m = 0.08 \cdot \exp(-V/11)$$

Slow Inward Current: I_{Ca}

$$I_{Ca} = g_{Ca,max} \cdot d \cdot f \cdot f_{Ca} \cdot (V - E_{Ca})$$

$$g_{Ca,max} = 0.064 \text{ mS}/\mu\text{F}$$

$$E_{Ca} = (RT/2F) \cdot \ln([Ca^{2+}]_o/[Ca^{2+}]_i)$$

$$\alpha_d = 14.98 / (16.68 \cdot \sqrt{2 \cdot \pi}) \exp\{-[(V - 22.36) / 16.68]^2 / 2\}$$

$$\beta_d = 0.1471 - 5.3 / (14.93 \cdot \sqrt{2 \cdot \pi}) \exp\{-[(V - 6.27) / 14.93]^2 / 2\}$$

$$\alpha_f = [6.87 \cdot 10^{-3}] / \{1 + \exp[(6.1546 - V) / -6.12]\}$$

$$\beta_f = \{0.069 \cdot \exp[-0.11 \cdot (V + 9.825)] + 0.011\} /$$

$$\{1 + \exp[-0.278 \cdot (V + 9.825)]\} - 5.75 \cdot 10^{-4}$$

$$f_{Ca} = 1 / (1 + ([Ca^{2+}]_i / K_{Ca}))$$

$$K_{Ca} = 600 \text{ nmol/L}$$

where $g_{Ca,max}$ is g_{max} for I_{Ca} , d is the activation gate of I_{Ca} , f is the inactivation gate of I_{Ca} , E_{Ca} is the equilibrium potential for Ca^{2+} , f_{Ca} is a proportional factor for Ca^{2+} -dependent inactivation of I_{Ca} , and K_{Ca} is half-maximum Ca^{2+} binding concentration for I_{Ca} .

Outward Current

Transient Outward Current: I_{to}

$$I_{to} = g_{to,max} \cdot r \cdot t \cdot (V - E_{to})$$

$$E_{to} = (RT/F) \cdot \ln\{(0.043 \cdot [Na^+]_o + [K^+]_o) / (0.043 \cdot [Na^+]_i + [K^+]_i)\}$$

$$g_{to,max}: \text{nonfailing} \geq 0.3 \text{ mS}/\mu\text{F}; \text{heart failure} \geq 0.191 \text{ mS}/\mu\text{F}$$

$$\alpha_r = \{0.5266 \cdot \exp[-0.0166 \cdot (V - 42.2912)]\} /$$

$$\{1 + \exp[-0.0943 \cdot (V - 42.2912)]\}$$

$$\beta_r = \{0.5149 \cdot \exp[-0.1344 \cdot (V - 5.0027)] + 5.186 \cdot 10^{-5} \cdot V\} /$$

$$\{1 + \exp[-0.1348 \cdot (V - 5.186 \cdot 10^{-5})]\}$$

$$\alpha_t = \{0.0721 \cdot \exp[-0.173 \cdot (V + 34.2531)] + 5.612 \cdot 10^{-5} \cdot V\} /$$

$$\{1 + \exp[-0.1732 \cdot (V + 34.2531)]\}$$

$$\beta_t = \{0.0767 \cdot \exp[-1.66 \cdot 10^{-9} \cdot (V + 34.0235)] + 1.215 \cdot 10^{-4} \cdot V\} /$$

$$\{1 + \exp[-0.1604 \cdot (V + 34.0235)]\}$$

where $g_{to,max}$ is g_{max} for I_{to} , r and t are the activation gate and the inactivation gate of I_{to} , respectively, and E_{to} is the equilibrium potential for I_{to} .

Delayed Rectifier Current

Slowly Activating Current: I_{Ks}

$$I_{Ks} = g_{Ks,max} \cdot X_s^2 \cdot (V - E_K)$$

$$E_{Ks} = (RT/F) \cdot \ln\{(0.01833 \cdot [Na^+]_o + [K^+]_o) / (0.01833 \cdot [Na^+]_i + [K^+]_i)\}$$

$$g_{Ks,max} = 0.02 \text{ mS}/\mu\text{F}$$

$$\alpha_{X_s} = 3.0 \cdot 10^{-3} / \{1 + \exp[(7.44 - (V+10)/14.32)]\}$$

$$\beta_{X_s} = 5.87 \cdot 10^{-3} / \{1 + \exp[(-5.95 - (V+10)/-15.82)]\}$$

where $g_{K_s, \max}$ is g_{\max} for I_{K_s} , X_s is the activation gate of I_{K_s} , and E_{K_s} is the equilibrium potential for I_{K_s} .

Rapidly Activating Current: I_{K_r}

$$I_{K_r} = g_{K_r, \max} \cdot X_r \cdot \text{rik} \cdot (V - E_K)$$

$$E_K = (RT/F) \cdot \ln([K^+]_o/[K^+]_i)$$

$$g_{K_r, \max} = 0.015 \text{ mS}/\mu\text{F}$$

$$\alpha_{X_r} = \{0.005 \cdot \exp[5.266 \cdot 10^{-4} \cdot (V+4.067)]\} / \{1 + \exp[-0.1262 \cdot (V+4.067)]\}$$

$$\beta_{X_r} = \{0.016 \cdot \exp[1.6 \cdot 10^{-3} \cdot (V+65.66)]\} /$$

$$\{1 + \exp[0.0783 \cdot (V+65.66)]\}$$

$$\text{rik} = 1 / \{1 + \exp[(V+26)/23]\}$$

where $g_{K_r, \max}$ is g_{\max} for I_{K_r} , X_r is the activation gate of I_{K_r} , rik is the inward-rectification factor of I_{K_r} , and E_K is the equilibrium potential for I_K .

Inward Rectifier Current: I_{K1}

$$I_{K1} = g_{K1, \max} \cdot K1_\infty \cdot (V - E_{K1})$$

$$E_{K1} = (RT/F) \cdot \ln([K^+]_o/[K^+]_i)$$

$$g_{K1, \max}: \text{nonfailing} \Rightarrow 2.5 \text{ mS}/\mu\text{F}; \text{ heart failure} \Rightarrow 2.0 \text{ mS}/\mu\text{F}$$

$$\alpha_{K1} = 0.1 / \{1 + \exp[0.06 \cdot (V - E_{K1} - 200)]\}$$

$$\beta_{K1} = \{3 \cdot \exp[2 \cdot 10^{-4} \cdot (V - E_{K1} + 100)] + \exp[0.1 \cdot (V - E_{K1} - 10)]\} /$$

$$\{1 + \exp[-0.5 \cdot (V - E_{K1})]\}$$

$$K1_\infty = \alpha_{K1} / (\alpha_{K1} + \beta_{K1})$$

where $g_{K1, \max}$ is g_{\max} for I_{K1} , $K1_\infty$ is the inactivation gate of I_{K1} , and E_{K1} is the equilibrium potential for I_{K1} .

Background Currents

Ca^{2+} Background Current: $I_{Ca,b}$

$$I_{Ca,b} = \bar{G}_{Ca,b} \cdot (V - E_{Ca,b})$$

$$\bar{G}_{Ca,b}: \text{nonfailing} \Rightarrow 0.00085 \text{ mS}/\mu\text{F}; \text{ heart failure} \Rightarrow 0.0013 \text{ mS}/\mu\text{F}$$

$$E_{Ca,b} = E_{Ca}$$

where $\bar{G}_{Ca,b}$ is g_{\max} for $I_{Ca,b}$, and $E_{Ca,b}$ is the equilibrium potential for $I_{Ca,b}$.

Na^+ Background Current: $I_{Na,b}$

$$I_{Na,b} = \bar{G}_{Na,b} \cdot (V - E_{Na,b})$$

$$\bar{G}_{Na,b}: \text{nonfailing} \Rightarrow 0.001 \text{ mS}/\mu\text{F}; \text{ heart failure} \Rightarrow 0 \text{ mS}/\mu\text{F}$$

$$E_{Na,b} = E_{Na}$$

where $\bar{G}_{Na,b}$ is g_{\max} for $I_{Na,b}$, and $E_{Na,b}$ is the equilibrium potential for $I_{Na,b}$.

Pump and Exchanger

$Na^+ - K^+$ Pump: I_{NaK}

$$I_{NaK} = \bar{I}_{NaK} \cdot f_{NaK} \cdot 1 / (1 + (K_{m,Na} / [Na^+]_i)^{1.5}) \cdot [[K^+]_o / ([K^+]_o + K_{m,Ko})]$$

$$\bar{I}_{NaK}: \text{nonfailing} \Rightarrow 1.3 \text{ pA}/\text{pF}; \text{ heart failure} \Rightarrow 0.75 \text{ pA}/\text{pF}$$

$$f_{NaK} = 1 / [1 + 0.1245 \cdot \exp(-0.1 \cdot V \cdot F/RT)]$$

$$+ 0.0365 \cdot \sigma \cdot \exp(-V \cdot F/RT)]$$

$$\sigma = 1/7 \cdot \{\exp([Na^+]_o/67.3) - 1\}$$

$$K_{m,Na} = 10 \text{ mmol}/L$$

$$K_{m,Ko} = 1.5 \text{ mmol}/L$$

where f_{NaK} is the voltage-dependence parameter of I_{NaK} , and σ is the $[Na^+]_o$ -dependence factor of I_{NaK} .

$Na^+ - Ca^{2+}$ Exchanger Current: I_{NaCa}

$$I_{NaCa} = k_{NaCa} \cdot (K_{m,Na}^3 + [Na^+]_o^3)^{-1} \cdot (K_{m,Ca} + [Ca^{2+}]_o)^{-1}$$

$$\cdot (1 + k_{sat} \cdot \exp[(\eta - 1) \cdot V \cdot F/(RT)])^{-1} \cdot \{\exp[\eta \cdot V \cdot F/(RT)]$$

$$\cdot [Na^+]_i^3 \cdot [Ca^{2+}]_o - \exp[(\eta - 1) \cdot V \cdot F/(RT)] \cdot [Na^+]_o^3 \cdot [Ca^{2+}]_i\}$$

$$k_{NaCa}: \text{nonfailing} \Rightarrow 1000 \text{ pA}/\text{pF}; \text{ heart failure} \Rightarrow 1650 \text{ pA}/\text{pF}$$

$$K_{m,Na} = 82.5 \text{ mmol}/L; K_{m,Ca} = 1.38 \text{ mmol}/L; k_{sat} = 0.1; \eta = 0.35$$

where k_{sat} is the saturation factor of I_{NaCa} at very negative potentials, and η is the position of the energy barrier controlling voltage dependence of I_{NaCa} .

Ca^{2+} Homeostasis

CICR of JSR

$$I_{rel} = G_{rel} ([Ca^+]_{JSR} - [Ca^{2+}]_i) \text{ in mmol}/L \text{ per ms}$$

$$G_{rel} = \bar{G}_{rel} \{ \Delta[Ca^{2+}]_{i,2} - \Delta[Ca^{2+}]_{i,th} / (K_{m,rel} + \Delta[Ca^{2+}]_{i,2} - \Delta[Ca^{2+}]_{i,th}) \}$$

$$\cdot (1 - \exp[-t/\tau_{on}]) \cdot \exp[-t/\tau_{off}]$$

$$\Delta[Ca^{2+}]_{i,2} = \Sigma \text{ calcium-influx during first 2 ms after initiation of AP}$$

$$\Delta[Ca^{2+}]_{i,th} = 0.005 \mu\text{mol}/L$$

$$K_{m,rel} = 0.8 \mu\text{mol}/L$$

$$\tau_{on} = \tau_{off} = 4 \text{ ms}; t=0 \text{ at time of CICR}$$

$$\bar{G}_{rel} = 22 \text{ ms}^{-1}$$

where I_{rel} is the SR Ca^{2+} release current, and G_{rel} is the rate constant of Ca^{2+} release from JSR.

Spontaneous Ca^{2+} Release of JSR

$$I_{rel} = G_{rel} ([Ca^{2+}]_{JSR} - [Ca^{2+}]_i) (1 - \exp[-t/\tau_{on}]) \cdot \exp[-t/\tau_{off}]$$

$$\text{in mmol}/L \text{ per ms}$$

$$G_{rel} = 3 \text{ ms}^{-1}$$

$$\tau_{on} = \tau_{off} = 4 \text{ ms}; t=0 \text{ at time of CICR}$$

Ca^{2+} Uptake and Leakage of NSR: I_{up} and I_{leak}

$$I_{up} = \bar{I}_{up} [Ca^{2+}]_i / ([Ca^{2+}]_i + K_{m,up}) \text{ in mmol}/L \text{ per ms}$$

$$I_{leak} = K_{leak} [Ca^{2+}]_{NSR} \text{ mmol}/L \text{ per ms}$$

$$\bar{I}_{up}: \text{nonfailing} \Rightarrow 0.0045; \text{ heart failure} \Rightarrow 0.0015 \text{ in mmol}/L \text{ per ms}$$

$$K_{m,up} = 0.92 \mu\text{mol}/L$$

$$K_{leak}: \text{nonfailing} \Rightarrow 0.00026 \text{ ms}^{-1}; \text{ heart failure} \Rightarrow 0.00017 \text{ ms}^{-1}$$

where I_{up} is the SR Ca^{2+} uptake current, and I_{leak} is the leakage current.

Translocation of Ca²⁺ From NSR to JSR: I_{tr}

$$I_{tr} = ([Ca^{2+}]_{NSR} - [Ca^{2+}]_{JSR}) / \tau_{tr} \text{ in mmol/L per ms}$$

$$\tau_{tr} = 180 \text{ ms}$$

where I_{tr} is the SR Ca²⁺ translocation current.

Ca²⁺ Buffers in the Myoplasm: Troponin (TRPN) and Calmodulin (CMDN)

$$\overline{[TRPN]} = \overline{[TRPN]} \{ [Ca^{2+}]_i / ([Ca^{2+}]_i + K_{m,TRPN}) \}$$

$$\overline{[CMDN]} = \overline{[CMDN]} \{ [Ca^{2+}]_i / ([Ca^{2+}]_i + K_{m,CMDN}) \}$$

$$\overline{[TRPN]} = 70 \mu\text{mol/L}$$

$$\overline{[CMDN]} = 50 \mu\text{mol/L}$$

$$K_{m,TRPN} = 0.5 \mu\text{mol/L}$$

$$K_{m,CMDN} = 2.38 \mu\text{mol/L}$$

where K_{m,TRPN} is the half-saturation concentration of TRPN, and K_{m,CMDN} is the half-saturation concentration of CMDN.

Ca²⁺ Buffer in JSR: Calsequestrin (CSQN)

$$\overline{[CSQN]} = \overline{[CSQN]} \{ [Ca^{2+}]_{JSR} / ([Ca^{2+}]_{JSR} + K_{m,CSQN}) \}$$

$$\overline{[CSQN]} = 10 \text{ mmol/L}$$

$$K_{m,CSQN} = 0.8 \text{ mmol/L}$$

where K_{m,CSQN} is the half-saturation concentration of CSQN.

Acknowledgments

This study was supported by the Deutsche Forschungsgemeinschaft (Be 1113/2–3) and the Bundesministerium für Bildung, Wissenschaft, Forschung und Technologie (01 Kans 9502). Special thanks go to Dr M. Lindner for recording the APs.

References

1. Kjekshus J. Arrhythmias and mortality in congestive heart failure. *Am J Cardiol.* 1990;65:421–481.
2. Pogwizd SM, Hoyt RH, Saffitz JE, Corr PB, Cox JL, Cain ME. Reentrant and focal mechanisms underlying ventricular tachycardia in the human heart. *Circulation.* 1992;86:1872–1887.
3. de Bakker JMT, Coronel R, Tasseron S. Ventricular tachycardia in the infarcted Langendorff perfused human heart: role of the arrangement of surviving cardiac fibers. *J Am Coll Cardiol.* 1990;15:1594–607.
4. de Bakker JMT, Van Capelle FJL, Janse MJ. Reentry as a cause of ventricular tachycardia in patients with chronic heart disease: electrophysiological and anatomic correlation. *Circulation.* 1988;77:589–606.
5. Gilmour JRF, Heger JJ, Prystowsky EN, Zipes DP. Cellular electrophysiologic abnormalities of diseased human ventricular myocardium. *Am J Cardiol.* 1983;51:137–144.
6. Wiederhold KF, Nilius B. Increased sensitivity of ventricular myocardium to intracellular calcium overload in Syrian cardiomyopathic hamster. *Biomed Biochim Acta.* 1986;45:1333–1337.
7. Nordin C, Gilat E, Aronson RS. Delayed afterdepolarizations and triggered activity in ventricular muscle from rats with streptozotocin-induced diabetes. *Circ Res.* 1985;57:28–34.
8. Aronson RS. Afterdepolarizations and triggered activity in hypertrophied myocardium from rats with renal hypertension. *Circ Res.* 1981;48:720–727.
9. January CT, Riddle JM, Salata JJ. A model for early afterdepolarizations: induction with the Ca²⁺ channel agonist Bay K 8644. *Circ Res.* 1988;62:563–571.
10. January CT, Riddle JM. Early afterdepolarizations: mechanism of induction and block: a role for L-type Ca²⁺ current. *Circ Res.* 1989;64:977–990.

11. Ferrier GL, Saunders JH, Mendez C. A cellular mechanism for the generation of ventricular arrhythmias by acetylstrophanthidin. *Circ Res.* 1973;32:600–689.
12. January CT, Fozzard HA. Delayed afterdepolarizations in heart muscle: mechanisms and relevance. *Pharmacol Rev.* 1988;40:219–227.
13. Beuckelmann DJ, Näbauer M, Erdmann E. Alterations of K⁺ currents in isolated human ventricular myocytes from patients with terminal heart failure. *Circ Res.* 1993;73:379–385.
14. Wettwer E, Amos G, Gath J, Zerkowski HR, Reidemeister JC, Ravens U. Transient outward current in human and rat ventricular myocytes. *Cardiovasc Res.* 1993;27:1662–1669.
15. Mewes T, Ravens U. L-type calcium currents of human myocytes from ventricle of non-failing and failing hearts and from atrium. *J Mol Cell Cardiol.* 1994;26:1307–1320.
16. Beuckelmann DJ, Näbauer M, Erdmann E. Characteristics of calcium-current in isolated human ventricular myocytes from patients with terminal heart failure. *J Mol Cell Cardiol.* 1991;23:929–937.
17. Cohen NM, Lederer WJ. Calcium current in single human cardiac myocytes. *J Cardiovasc Electrophysiol.* 1993;4:422–437.
18. Oquadid H, Albat B, Nargeot J. Calcium currents in diseased human cardiac myocytes. *J Cardiovasc Pharmacol.* 1995;25:282–291.
19. Näbauer M, Beuckelmann DJ, Erdmann E. Characteristics of transient outward current in human ventricular myocytes from patients with terminal heart failure. *Circ Res.* 1993;73:386–394.
20. Näbauer M, Beuckelmann DJ, Überfuhr P, Steinbeck G. Regional differences in current density and rate-dependent properties of the transient outward current in subepicardial and subendocardial myocytes of human left ventricle. *Circulation.* 1996;93:168–177.
21. Li GR, Feng J, Yue L, Carrier M, Nattel S. Evidence for two components of delayed rectifier K⁺ current in human ventricular myocytes. *Circ Res.* 1996;78:689–696.
22. Koumi S, Backer CL, Arentzen CE. Characterization of inwardly rectifying K⁺ channel in human cardiac myocytes. Alterations in channel behavior in myocytes isolated from patients with idiopathic dilated cardiomyopathy. *Circulation.* 1995;92:164–174.
23. Bénitah JP, Bailly P, D'Agrosa MC, Da P, Delgado C, Lorente P. Slow inward current in single myocytes isolated from adult human ventricles. *Pflügers Arch.* 1992;421:176–187.
24. Veldkamp MW, van Ginneken AC, Opthof T, Bouman LN. Delayed rectifier channels in human ventricular myocytes. *Circulation.* 1995;92:3497–3504.
25. Sakakibara Y, Furukawa T, Singer DH, Jia H, Backer CL, Arentzen CE, Wasserstrom JA. Sodium current in isolated human ventricular myocytes. *Am J Physiol.* 1993;265:H1301–H1309.
26. Gwathmey JK, Copelas L, MacKinnon R, Schoen FJ, Feldman MD, Grossman W, Morgan JP. Abnormal intracellular calcium handling in myocardium from patients with end-stage heart failure. *Circ Res.* 1987;61:70–76.
27. Beuckelmann DJ, Näbauer M, Erdmann E. Intracellular calcium handling in isolated ventricular myocytes from patients with terminal heart failure. *Circulation.* 1992;85:1046–1055.
28. Reinecke H, Studer R, Vetter R, Holtz J, Drexler H. Cardiac Na⁺/Ca²⁺ exchange activity in patients with end-stage heart failure. *Cardiovasc Res.* 1996;31:48–54.
29. Flesch M, Schwinger RHG, Schiffer F, Frank K, Südkamp M, Kuhn-Regnier F, Arnold G, Böhm M. Evidence for functional relevance of an enhanced expression of the Na⁺-Ca²⁺ exchanger in failing human myocardium. *Circulation.* 1996;94:992–1002.
30. Hodgkin AL, Huxley AF. A quantitative description of membrane current and its application to conduction and excitation in nerve. *J Physiol (Lond).* 1952;117:500–544.
31. Luo C-H, Rudy Y. A dynamic model of the cardiac ventricular action potential, I: simulations of ionic currents and concentration changes. *Circ Res.* 1994;74:1071–1096.
32. Sipido KR, Callewaert G, Carmeliet E. Inhibition and rapid recovery of Ca²⁺ current during Ca²⁺ release from sarcoplasmic reticulum in guinea pig ventricular myocytes. *Circ Res.* 1995;76:102–109.
33. De Leon M, Wang Y, Jones L, Perez-Reyes E, Wei X, Wah Soong T, Snutch TP, Yue DT. Essential Ca²⁺-binding motif for Ca²⁺-sensitive inactivation of L-type Ca²⁺ channels. *Science.* 1995;270:1502–1505.
34. Sanguinetti MC, Jurkiewicz NK. Two components of cardiac delayed rectifier K⁺ current: differential sensitivity to block by class III antiarrhythmic agents. *J Gen Physiol.* 1990;96:195–215.

35. Splawski I, Tristani-Firouzi M, Lehmann MH, Sanguinetti MC, Keating MT. Mutations in the hmnk gene cause long QT syndrome and suppress I_{Ks} function. *Nat Genet.* 1997;17:338–340.
36. Those N. Calcium-sensitive delayed rectifier potassium current in guinea pig ventricular cells. *Am J Physiol.* 1990;258:H1200–H1207.
37. Sanguinetti MC, Jurkiewicz NK. Role of external Ca^{2+} and K^{+} in gating of cardiac delayed rectifier K^{+} currents. *Pflugers Arch.* 1992;420:180–186.
38. Sham JSK, Hatem SN, Morad M. Species differences in the activity of the Na^{+} - Ca^{2+} exchanger in mammalian cardiac myocytes. *J Physiol (Lond).* 1995;488:3:623–631.
39. Peeters GA, Sanguinetti MC, Eki Y, Konarzewska H, Renlund DG, Karwande SV, Barry WH. Method for isolation of human ventricular myocytes from single endocardial and epicardial biopsies. *Am J Physiol.* 1995;268:H1757–H1764.
40. Shamraj OI, Grupp IL, Grupp G, Melvin D, Gradoux N, Kremers W, Lingrel JB, De Pover A. Characterisation of Na/K-ATPase, its isoforms, and the inotropic response to ouabain in isolated failing human hearts. *Cardiovasc Res.* 1993;27:2229–2237.
41. Holmberg SR, Williams AJ. The calcium-release channel from cardiac sarcoplasmic reticulum: function in the failing and acutely ischemic heart. *Circ Res.* 1989;65:1445–1449.
42. Schumacher C, Konigs B, Sigmund M, Kohne B, Schondube F, Vob M, Stein B, Weil J, Hanrath P. The ryanodine binding sarcoplasmic reticulum calcium release channel in nonfailing and in failing human myocardium. *Naunyn Schmiedeberg's Arch Pharmacol.* 1995;353:80–85.
43. Gwathmey JK, Hajjar RJ. Relation between steady-state force and intracellular $[Ca^{2+}]_i$ in intact human myocardium: index of myofibrillar responsiveness to Ca^{2+} . *Circulation.* 1990;82:1266–1278.
44. Meyer M, Schillinger W, Pieske B, Holubarsch C, Heilmann C, Posival H, Kuwajima G, Mikoshiha K, Just H, Hasenfuss G. Alterations of sarcoplasmic reticulum proteins in failing human dilated cardiomyopathy. *Circulation.* 1995;92:778–784.
45. Hilgemann DW, Noble D. Excitation-contraction coupling and extracellular calcium transients in rabbit atrium: reconstruction of basic cellular mechanism. *Proc R Soc Lond.* 1987;230:163–205.
46. Schwinger RH, Böhm M, Schmidt U, Karczewski P, Bavendiek U, Flesch M, Krause EG, Erdmann E. Unchanged protein levels of SERCA II and phospholamban but reduced Ca^{2+} uptake and Ca^{2+} -ATPase activity of cardiac sarcoplasmic reticulum from dilated cardiomyopathy patients compared with patients with nonfailing hearts. *Circulation.* 1995;92:3220–3228.
47. Hasenfuss G, Reinecke H, Studer R, Meyer M, Pieske B, Holtz J, Holubarsch C, Posival H, Just H, Drexler H. Relation between myocardial function and expression of sarcoplasmic reticulum Ca^{2+} -ATPase in failing and nonfailing human myocardium. *Circ Res.* 1994;75:434–442.
48. Beuckelmann DJ, Näbauer M, Krüger C, Erdmann E. Altered diastolic $[Ca^{2+}]_i$ handling in human ventricular myocytes from patients with terminal heart failure. *Am Heart J.* 1995;129:684–689.
49. Lindner M, Erdmann E, Beuckelmann DJ. Calcium content of the sarcoplasmic reticulum in isolated ventricular myocytes from patients with terminal heart failure. *J Mol Cell Cardiol.* In press.
50. Coltart DJ, Meldrum SJ. Hypertrophic cardiomyopathy: an electrophysiological study. *Br Med J.* 1970;4:217–218.
51. Morgan JM, Cunningham D, Rowland E. Electrical restitution in the endocardium of the intact human right ventricle. *Br Heart J.* 1992;67:42–46.
52. Franz MR, Swerdlow CD, Liem LB, Schaefer J. Cycle length dependence of human action potential duration in vivo: effects of single extrastimuli, sudden sustained rate acceleration and deceleration, and different steady-state frequencies. *J Clin Invest.* 1988;82:972–979.
53. Berger F, Borchard U, Hafner D, Kammer T, Weis T. Modulation of action potential duration by inhibition of the transient outward current in sheep cardiac Purkinje fibers. *Basis Res Cardiol.* 1995;90:185–191.
54. Käab S, Nuss HB, Chiamvimonvat N, O'Rourke B, Pak PH, Kass DA, Marban E, Tomaselli GF. Ionic mechanism of action potential prolongation in ventricular myocytes from dogs with pacing-induced heart failure. *Circ Res.* 1996;78:262–273.
55. Navarro-Polanco RA, Sanchez-Chapula JA. 4-Aminopyridine activates potassium currents by activation of a muscarinic receptor in feline atrial myocytes. *J Physiol (Lond).* 1997;498:3:663–678.
56. Zeng J, Laurita KR, Rosenbaum DS, Rudy Y. Two components of the delayed rectifier K^{+} current in ventricular myocytes of the guinea pig type: theoretical formulation and their role in repolarization. *Circ Res.* 1995;77:140–152.
57. Huikuri HV, Yli-Mayry S. Frequency dependent effects of d-sotalol and amiodarone on the action potential duration of the human right ventricle. *Pacing Clin Electrophysiol.* 1992;15:2103–2107.
58. Hayward RP, Taggart P. Effect of sotalol on human atrial action potential duration and refractoriness: cycle length dependency of class III activity. *Cardiovasc Res.* 1986;20:100–107.
59. Newman D, Dorian P, Feder-Elituv R. Isoproterenol antagonizes drug-induced prolongation of action potential duration in humans. *Can J Physiol Pharmacol.* 1993;71:755–760.
60. Carlsson L, Abrahamsson C, Almgren O, Lundberg C, Duker G. Prolonged action potential duration and positive inotropy induced by the novel class III antiarrhythmic agent H 234/09 (almokalant) in isolated human ventricular muscle. *J Cardiovasc Pharmacol.* 1991;18:882–887.
61. Wettwer E, Grundke M, Ravens U. Differential effects of the new class III antiarrhythmic agents almokalant, E-4031 and D-sotalol, and of quinidine, on delayed rectifier currents in guinea pig ventricular myocytes. *Cardiovasc Res.* 1992;26:1145–1152.
62. Fedida D, Noble D, Rankin AC, Spindler AJ. The arrhythmogenic transient inward current I_{ti} and related contraction in isolated guinea-pig ventricular myocytes. *J Physiol (Lond).* 1987;392:523–542.
63. Giles W, Shimoni Y. Comparison of sodium-calcium exchanger and transient inward currents in single cells from rabbit ventricle. *J Physiol (Lond).* 1989;417:465–481.
64. Luo CH, Rudy Y. A model of the ventricular cardiac action potential. Depolarization, repolarization, and their interaction. *Circ Res.* 1991;68:1501–1526.
65. Yue L, Feng J, Li GR, Nattel S. Transient outward and delayed rectifier currents in canine atrium: properties and role of isolation methods. *Am J Physiol.* 1996;270:H2157–H2168.
66. Thuringer D, Deroubaix E, Coulombe A, Coraboeuf E, Mercadier JJ. Ionic basis of the action potential prolongation in ventricular myocytes from Syrian hamsters with dilated cardiomyopathy. *Cardiovasc Res.* 1996;31:747–757.
67. Cerbai E, Barbieri M, Li Q, Mugelli A. Ionic basis of action potential prolongation of hypertrophied cardiac myocytes isolated from hypertensive rats of different ages. *Cardiovasc Res.* 1994;28:1180–1187.
68. Nygren A, Fiset C, Clark JW, Lindblad DS, Clark RB, Giles WR. Mathematical model of an adult human atrial cell: the role of K^{+} currents in repolarization. *Circ Res.* 1998;82:63–81.
69. Firek L, Giles WR. Outward currents underlying repolarization in human atrial myocytes. *Cardiovasc Res.* 1995;30:31–38.
70. Stern MD, Capogrossi MC, Lakatta EG. Spontaneous calcium release from the sarcoplasmic reticulum in myocardial cells: mechanisms and consequences. *Cell Calcium.* 1988;9:247–256.
71. Capogrossi MC, Houser SR, Bahinski A, Lakatta EG. Synchronous occurrence of spontaneous localized calcium release from the sarcoplasmic reticulum generates action potentials in rat cardiac ventricular myocytes at normal resting membrane potential. *Circ Res.* 1987;61:498–503.
72. Aronson RS. Afterdepolarizations and triggered activity in hypertrophied myocardium from rats with renal hypertension. *Circ Res.* 1981;48:720–727.
73. Vermeulen JT, McGuire MA, Opthof T, Coronel R, de Bakker JMT, Klöpping C, Janse MJ. Triggered activity and automaticity in ventricular trabeculae of failing human and rabbit hearts. *Cardiovasc Res.* 1994;28:1547–1554.
74. Ehara T, Noma A, Ono K. Calcium-activated non-selective cation channels in ventricular cells isolated from adult guinea-pig hearts. *J Physiol (Lond).* 1988;403:117–133.
75. Cannell MB, Lederer WJ. The arrhythmogenic current I_{ti} in the absence of electrogenic sodium-calcium exchange in sheep cardiac Purkinje fibres. *J Physiol (Lond).* 1986;374:201–219.
76. Luo CH, Rudy Y. A dynamic model of the cardiac ventricular action potential. II: afterdepolarizations, triggered activity, and potentiation. *Circ Res.* 1994;74:1097–1113.
77. Nordin C, Ming Z. Computer model of current-induced early afterdepolarizations in guinea pig ventricular myocytes. *Am J Physiol.* 1995;268:H2440–H2459.
78. Zeng J, Rudy Y. Early afterdepolarizations in cardiac myocytes: mechanism and rate dependence. *Biophys J.* 1995;68:949–964.

79. Cranfield PF, Aronson RS. *Cardiac Arrhythmias: The Role of Triggered Activity and Other Mechanisms*. New York, NY: Futura Publishing Co Inc; 1988.
80. Keung EC, Aronson RS. Nonuniform electrophysiological properties and electrotonic interaction in hypertrophied rat myocardium. *Circ Res*. 1981; 49:150–158.
81. Aronson RS, Ming Z. Cellular mechanisms of arrhythmias in hypertrophied and failing myocardium. *Circulation*. 1993;87[suppl VII]:VII-76–VII-83.
82. Gintant GA. Regional differences in I_K density in canine left ventricle: role of I_{Ks} in electrical heterogeneity. *Am J Physiol*. 1995;268:H604–H613.
83. Drouin E, Charpentier F, Gauthier C, Laurent K, Le Marec H. Electrophysiologic characteristics of cells spanning the left ventricular wall of human heart: evidence for presence of M cells. *J Am Coll Cardiol*. 1995;26:185–192.
84. Keung ECH, Keung CS, Aronson RS. Passive electrical properties of normal and hypertrophied rat myocardium. *Am J Physiol*. 1982;243:H917–H926.
85. Nordin C. Computer model of membrane current and intracellular Ca^{2+} flux in the isolated guinea pig ventricular myocyte. *Am J Physiol*. 1993; 265:H2117–H2136.
86. DiFrancesco D, Noble D. A model of cardiac electrical activity incorporating ionic pumps and concentration changes. *Philos Trans R Soc Lond*. 1985;307:353–398.
87. Rasmusson RL, Clark JW, Giles WR, Robinson K, Clark RB, Shibata EF, Campbell DL. A mathematical model of electrophysiological activity in a bullfrog atrial cell. *Am J Physiol*. 1990;259:H370–H389.
88. Lindblad DS, Murphey CR, Clark JW, Giles WR. A model of the action potential and underlying membrane currents in a rabbit atrial cell. *Am J Physiol*. 1996;271:H1666–H1696.
89. Shaw RB, Rudy Y. Electrophysiologic effects of acute myocardial ischemia: a theoretical study of altered cell excitability and action potential duration. *Cardiovasc Res*. 1997;35:256–272.